2011
2012

GENEESKUNDE

master in de biomedische wetenschappen: bio-elektronica en nanotechnologie

Masterproef

Nanostructures as platform for biosensors

Promotor :
dr. Anitha ETHIRAJAN

Copromotor :
Prof. dr. Hans-Gerhard BOYEN

Tanya Jacobs

Masterproef voorgedragen tot het bekomen van de graad van master in de biomedische wetenschappen , afstudeerrichting bio-elektronica en nanotechnologie

Maastricht University

universiteit hasselt
KNOWLEDGE IN ACTION

De transnationale Universiteit Limburg is een uniek samenwerkingsverband van twee universiteiten in twee landen: de Universiteit Hasselt en Maastricht University

universiteit hasselt
KNOWLEDGE IN ACTION

Maastricht University

Universiteit Hasselt | Campus Diepenbeek | Agoralaan Gebouw D | BE-3590 Diepenbeek
Universiteit Hasselt | Campus Hasselt | Martelarenlaan 42 | BE-3500 Hasselt

2011
2012

GENEESKUNDE

master in de biomedische wetenschappen: bio-elektronica en nanotechnologie

Masterproef

Nanostructures as platform for biosensors

Promotor :
dr. Anitha ETHIRAJAN

Copromotor :
Prof. dr. Hans-Gerhard BOYEN

Tanya Jacobs

Masterproef voorgedragen tot het bekomen van de graad van master in de biomedische wetenschappen , afstudeerrichting bio-elektronica en nanotechnologie

Maastricht University

universiteit hasselt
KNOWLEDGE IN ACTION

Table of Content

Abbreviations

AFM	:	Atomic Force Microscope
AC	:	Alternating Current
cDNA	:	Complementary DNA
CMC	:	Critical Micelle Concentration
DGGE	:	Denaturation Gradient Gel Electrophoresis
dsDNA	:	Double Stranded DNA
EDC	:	1-ethyl-3-(3-dimethylaminopropyl)-carbodiimide
EIS	:	Electrochemical Impedance Spectroscopy
FWHM	:	Full Width Half Maximum
HCl	:	Hydrogen Chloride
H_2O_2	:	Hydrogen Peroxide
IMO	:	Institute for Materials Research
NaOH	:	Sodium Hydroxide
NH_4OH	:	Ammonium Hydroxide
P2VP	:	Poly-2-VinylPyridine
PBS	:	Phosphate Buffered Saline
PCR	:	Poly Chain Reaction
PS	:	Poly Styrene
PS(x)-*b*-P2VP(y)	:	Poly Styrene(x)-*block*-Poly-2-VinylPyridine(y)
RT	:	Room Temperature
R_{th}	:	Thermal Resistance
SDS	:	Sodium Dodecyl Sulphate
SH	:	Thiol
Si	:	Silicon
SNP	:	Single Nucleotide Polymorphism
SPR	:	Surface Plasmon Resonance
SSC	:	Sodium Chloride Sodium Citrate
Ta_2O_5	:	Tantalum pentoxide
XPS	:	X-ray Photoelectron Spectroscopy

Acknowledgement

I would like to thank Prof. Dr. Patrick Wagner (BIOSensor group), Dr. Anitha Ethirajan (BIOSensor group) and Prof. Dr. Hans-Gerd Boyen (Nanostructure Physics group) for making it possible for me to do my master thesis in such an interesting interdisciplinary topic at the Institute of Materials Research (IMO).

From the Nanostructure Physics group I also want to thank Sathya Punniyakoti for the support during sample preparation. By etching samples, characterizing them with AFM and performing surface scans on them with XPS, he made sure I could work with samples of an outstanding quality. I would also like to thanks Prof. Dr. Hans-Gerd Boyen, because of his support with the XPS studies.

Regarding the BIOSensor group I would also like to thank a few people. First of all Bart van Grinsven for teaching me how to work with his electrochemical impedance analyzer and supporting me with analyzing EIS data. Also, I would like to thank Lars Grieten for explanations about the Iviumstat and the HP 4194A impedance/gain-phase analyzer.

My thanks also go out to all the other researchers of the above mentioned groups for considering me a part of the group and to Johnny Baccus for his technical support.

I would also like to thank Ruben Lanche and Brecht Billen for reading and commenting on my written thesis.

Last but not least I would like to thank my promoter Dr. Anitha Ethirajan for her guidance during the master thesis.

Abstract – English

The detection of specific DNA sequences is useful for the detection of pathogens responsible for diseases and as a preventive technique by checking water or food supplies for certain pathogens. The detection of specific DNA sequences is also important in gene expression studies and for the detection of mutations in the genome. Expensive, time-consuming and multi-step techniques are currently used for detecting specific DNA sequences. Some examples are denaturation gradient gel electrophoresis (DGGE), Southern blotting and micro arrays. For these optical techniques labeling or staining is required to visualize the result. Another possible technique is surface plasmon resonance (SPR), for this technique no labeling is required, but miniaturization is hard to achieve. Current biosensor research at the Institute of Materials Research focusses on a diamond-based setup, where a lengthy fatty acid technique is combined with EDC-coupling and aggressive cleaning procedures. Therefore this research aims to create a sensitive and selective biosensor which overcomes the before mentioned drawbacks. To create nanoparticle arrays for biosensing, without the need for a linker molecule when attaching DNA, nor the need for long and complex preparation procedures and labeling. A biosensor which can be miniaturized to a hand-held device for point-of-care testing.

Nanoparticles, made by the micellar approach, are obtained by plasma etching of the metal salt loaded micelles deposited on a substrate (silicon, tantalum pentoxide and diamond). DNA will be attached to the gold nanoparticles by physical absorption. The SH-group of SH-terminated DNA has a pronounced affinity for gold and binding will occur spontaneously. Therefore no complex chemistry is needed to create this link. To avoid the use of labeled probes or enzymes, electrochemical impedance spectroscopy (EIS) will be used as an in real-time detection technique. This is the first time that the micellar approach, physical absorption and EIS are combined to create a biosensor setup.

This master thesis proves that by combining the micellar approach, physical absorption of DNA and EIS, a fast and easy method for the detection of specific DNA sequences can be made. A biosensor based on nanostructures will allow miniaturization of the sensor and also massive parallel screening at the point-of-care.

Abstract – Nederlands

De detectie van specifieke DNA sequenties is nuttig bij het opsporen van pathogenen die ziekte veroorzaken en als een preventieve techniek door het controleren van water- en voedselvoorraden op zekere pathogenen. De detectie van specifieke DNA sequenties is ook belangrijk bij genexpressie studies en bij het opsporen van mutaties in het genoom. Dure, tijdrovende en meerstappen technieken worden momenteel gebruikt voor het opsporen van specifieke DNA sequenties. Denaturerende gradiënt gel elektroforese (DGGE), Southern blotting en micro arrays zijn enkele voorbeelden hiervan. Voor deze optische technieken is het noodzakelijk te labelen of te kleuren om het resultaat te visualiseren. Een andere mogelijke techniek ter detectie van DNA sequenties is oppervlakte plasmon resonantie (SPR). Voor deze techniek is labelen of kleuren van het DNA niet nodig, maar miniaturisatie van de techniek is zeer moeilijk. Huidig onderzoek naar biosensoren bij het Instituut voor Materiaalonderzoek focust zich op een sensor met een diamanten substraat, waarbij een vetzuurkoppeling gecombineerd wordt met EDC-koppeling en agressieve reinigings-procedures. Om al de genoemde nadelen te overkomen wordt er tijdens dit onderzoek een sensitieve en selectieve biosensor gemaakt, waarbij een nanopartikel array voor biosensing wordt gecreëerd, zonder gebruik te maken van linkermoleculen wanneer DNA wordt gebonden aan de partikels, noch gebruik te maken van lange en complexe procedures, noch labelen of kleuren van DNA. Een biosensor die geminimaliseerd kan worden naar een draagbaar toestel voor point-of-care metingen.

Nanopartikels, gemaakt door de micellaire aanpak, worden verkregen door het plasma etsen van de micellen (geladen met metaalzout) aanwezig op een substraat (silicium, tantalum pentoxide of diamant). DNA wordt op de gouden partikels gebonden door fysische absorptie. De SH-groep van SH-getermineerd DNA heeft een uitgesproken affiniteit voor goud en de binding zal spontaan ontstaan, waardoor er geen complexe chemie nodig is om deze binding te creëren. Om het gebruik van labels of enzymen te vermijden wordt elektrochemische impedantie spectroscopie (EIS) gebruikt als een in real time detectie techniek. Dit is de eerste keer dat de micellaire aanpak, fysische absorptie en EIS worden gecombineerd om een biosensor te maken.

Deze masterthesis bewijst dat door deze combinatie een snelle en gemakkelijk te gebruiken methode voor de detectie van specifieke DNA sequenties kan worden gemaakt. Een biosensor gebaseerd op nanopartikels laat miniaturisatie toe, waardoor parallelle screening op de point-of-care mogelijk wordt.

1) Introduction

The detection of specific DNA sequences is very relevant in the field of medical diagnostics and forensic sciences. Detection of specific DNA sequences is also important for food and environmental safety. Pathogens responsible for diseases can be detected by using their unique nucleic acid sequence. Detection of the pathogens can help in finding the appropriate treatment for a patient. The detection of specific DNA is also important in gene expression studies. Gene expression studies can be performed to study the activity of genes in a single sample or to compare the expression in two samples, for instance healthy and diseased tissue. In mutation research the detection of specific DNA sequences is also critical. Detection of specific DNA sequences can also be used as a preventive technique by checking water or food supplies for certain pathogens.

Currently time-consuming, multi-step and often expensive techniques are used for detecting specific DNA sequences. Some examples are denaturation gradient gel electrophoresis[1], Southern blotting[2] and micro arrays[3]. Another downside of these optical techniques is that labeling or staining is required. Surface plasmon resonance (SPR)[4] is a real-time, optical technique that does not require labeling or staining. SPR is a well-established technique in the life-science sector. It provides information on, for instance, binding affinity, analyte concentration and molecule detection. Although SPR is widely spread and is also accepted as a bench mark technique by many researchers, the main drawback of this technique is that it is difficult to miniaturize into a hand-held device.

Within Institute of Materials Research (IMO) at UHasselt, the label free detection of single nucleotide polymorphisms (SNP's) studying double stranded (ds)DNA stability is an active research area. A remarkable breakthrough has been recently achieved in determining the SNP's using impedance spectroscopy employing diamond based sensor electrodes.[5] The probe DNA is covalently coupled to the diamond substrate via a linker molecule (unsaturated fatty acid) that is photochemically attached to the H-terminated diamond. For the functionalization of the substrate with probe DNA, 1-ethyl-3-(3-dimethylaminopropyl)-carbodiimide (EDC)-coupling between the fatty acids and probe DNA is performed. At last the probe DNA is hybridized with different types of complementary DNA (cDNA). The used cDNA for a typical experiment consists of complementary, random and single mismatches at two different positions. The samples are then further used for electronic monitoring of chemically induced denaturation of different dsDNA at room temperature using impedance spectroscopy.

Although the novel detection technique itself is fast, highly efficient and simple, the sample preparation time is quite long. Photochemical attaching of fatty acids to H-terminated diamond is a lengthy procedure requiring minimum 20 hours followed by washing with acetic acid to remove unbound fatty acids. But then the substrate is not yet functionalized with probe DNA; EDC coupling is required to attach probe DNA. Although each sample can be used for a series of impedance measurements, in any case prior to the measurements it has to go through an aggressive cleaning procedure with sulphuric acid and potassium nitrate. In

general it can be concluded that to make such a biosensor a lengthy procedure and complicated chemistry is needed.

This research aims to extend the above mentioned technique of electronic monitoring of chemically induced denaturation of DNA duplexes by employing a sensitive and selective biosensor which overcomes the before mentioned drawbacks. This hand-held biosensor should be able to do fast and massive parallel screening at the point-of-care. A nanoparticle array for biosensing will be created, without the need for a linker molecule when attaching DNA, nor the need for long and complex sample preparation procedures.

The production of inorganic nanoparticles has drawn our attention because of their interesting physical and chemical properties arising due to the quantum confinement effect.[6-8] Gold particles for targeted drug delivery[9], quantum dots for medical imaging[10], palladium nanoparticles-based hydrogen sensor[11], diagnostic testing using gold nanoparticles to detect low levels of proteins indicating particular diseases[12] are just a few examples of the applications of nanoparticles. Nanoparticles are a good platform for biosensing, which can be used as immobilization platform for DNA or proteins. The high surface-to-volume ratio of nanoparticles enlarges the surface area of the biosensor and therefore an increase in bound molecules can be expected, which will have an effect on the sensitivity of a biosensor.[8] Nanoparticles can not only be used as an immobilization platform for biosensing but can also be used for sensing with techniques that can monitor changes in electronic properties of the nanoparticles; the latter behavior is for instance used in SPR-measurements. Another benefit of nanoparticles is that they will allow miniaturization of biosensors. Because of this miniaturization massive parallel screening will still be possible on a point-of-care biosensor.

The use of metal nanoparticles as immobilization platform is not a new concept. Several research groups[13-15] uses the affinity of thiolated (SH)-DNA to create a specific binding with gold nanoparticles. Physical absorption allows binding of SH-terminated DNA to gold without extra preparation of the surface. There are also no linker molecules needed to attach the probe DNA. After attaching probe DNA it can be hybridized with its complementary strand. Denaturation of DNA can then be studied due to an optical change during this process or by an electrical measuring technique, such as electrochemical impedance spectroscopy (EIS)[16]. EIS measures the change in electrical resistance (impedance) at alternating current. Not only the attachment of probe DNA, but also the hybridization and denaturation of the DNA-strands with complementary DNA can be studied with EIS.[5, 17, 18] EIS is a promising technique in the field of molecular diagnostics because it is label-free, fast and it can be used for real-time measurements. Due to the effectiveness and efficiency of the EIS technique and that the devices using EIS can be miniaturized, EIS will be used as read-out technique for this research.

A highly ordered array of nanoparticles is needed to guarantee the quality of the biosensor and repeatability of the measurements with this biosensor. Nanoparticles can be made in different ways, for example by wet-chemical procedures at elevated temperatures (for instance arrested nucleation and growth[19]) or they can be formed in cluster beams[20]. A drawback of these

techniques is that the nanoparticles can aggregate during heat treatments. To stop aggregation and to get an ordered organization, the particles need to be encapsulated with a stabilizing agent, for example an organic-ligand shell. This can be done either after deposition from a cluster beam or during synthesis.[21] The surface will therefore be covered with a ligand shell thereby affecting the attachment of biomolecules on to the surface of the nanoparticle. The micellar approach that will be used to make metal nanoparticles during this research does not show these drawbacks. The micellar approach provides size-selected, separated, atomically clean, hexagonally ordered nanoparticles supported on suitable substrates.[22]

This is the first time that the micellar approach will be used to produce gold nanoparticles that can be used for physical absorption of probe DNA and further used for dsDNA denaturation studies employing EIS. The combination of these techniques will allow the creation of a fast and easy to use biosensor to detect specific DNA sequences and SNP's. The use of linker molecules, long preparation times and the need for complex chemistry can be excluded. Additionally, a nanoparticle array based sensor is a big step towards the miniaturization of the biosensor platform which could be employed for massive screening at the point-of-care.

1.1) Micellar approach

A micelle is an aggregate of amphiphilic molecules dispersed in a liquid. An amphiphilic molecule contains two components (figure 1A). The hydrophilic part has an affinity for polar solvents and the hydrophobic part has an affinity for apolar solvents. Amphiphilic molecules such as in soaps or detergents, arrange themselves at the surface of the solution (figure 1B) or form micelles within the solution (figure 1C). Micelle formation is a balanced reaction and the amphiphilic molecules switch places continuously. The concentration of the amphiphilic molecule decides the portion of molecules that are present at the surface or as micelles. At low concentration amphiphiles will favor arrangement at the surface of the solution. At higher concentrations of amphiphilic molecules the surface becomes saturated and micelles are formed. This concentration of amphiphilic molecules is called the critical micelle concentration (CMC) (figure 1D).[23, 24]

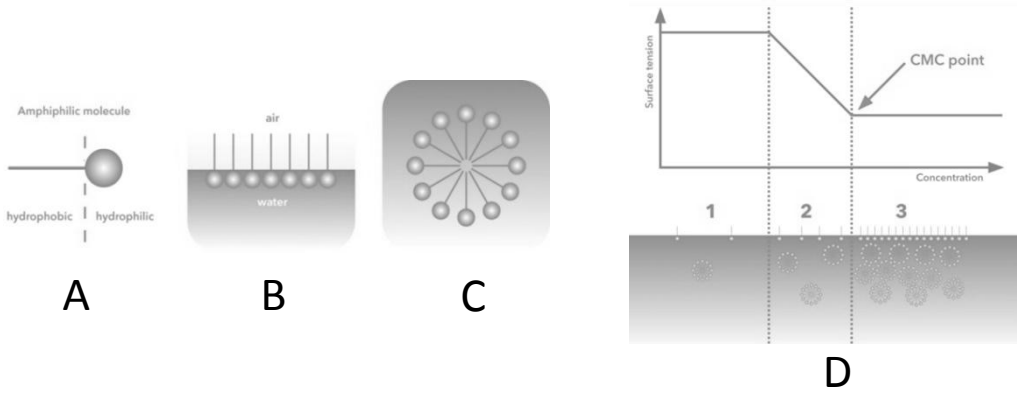

Figure 1: Amphiphilic molecules and the arrangement in a polar solvent. A: amphiphilic molecule, B: arrangement of molecules at the surface, C: arrangement of molecules in to micelles, D: critical micelle concentration (CMC). Picture from: http://www.attension.com/critical-micelle-concentration.aspx.

The micellar approach is a two-step process. First reversed micelles are formed by the self-organization of macromolecules (such as: polystyrene(x)-*block*-poly-2-vinylpyridine(y) (PS(x)-*b*-P2VP(y)) (figure 2), in an apolar solvent. Secondly, the reversed micelles provide nanosized compartments for the loading of metal salts.[22] The amount of metal salt ($HAuCl_4$) to add to the solution can be calculated using equation 1. The metal salt migrates to the core of the reversed micelles when softly stirred. When the solution is at equilibrium all the micelles will be loaded with the same amount of metal salt, leading to a small size distribution of the resulting salt loaded micelles. To reach the equilibrium stirring the solution can take up as much as 21 days for high molecular weight polymers such as PS(185000)-*b*-P2VP(90000). It should be noted here that polymers with lower molecular weight, such as PS(32500)-*b*-P2VP(7800), can be ultrasonicated for a few hours to reach equilibrium.

$$Amount\ of\ salt\ to\ add = \frac{Polymer\ Amount}{MW(PS) + MW(P2VP}\ x\ \frac{MW(P2VP)}{MM\ (P2VP)}\ x\ MM(HAuCl_4) x\ LR$$

Equation 1: Amount of metal salt to be added to the solution for a metal salt : nitrogen ratio of 0.5. In this formula the metal salt is $HAuCl_4$. This loading ratio (LR) can be adjusted to alter the salt loading. MW= molecular weight, MM= molecular mass.

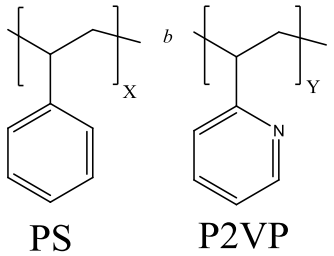

Figure 2: Diblock polymer polystyrene(X)-*b*-poly-2-vinylpyridine(Y). The number in brackets give the molecular weight of the blocks.

The salt-loaded micelles are dip-coated on a substrate. During dip-coating the micelles form a monolayer with a hexagonal arrangement. For high molecular weight polymers a higher dip-coating speed (here 14 mm/min) needs to be used, while for polymers with a lower molecular weight dip-coating is performed at a speed of 6 mm/min.[25] As long as the toluene on the dip-coated sample has not dried, it is possible for the micelles to migrate to more energy favorable positions. The dip-coated samples are characterized with the atomic force microscope (AFM). To form the nanoparticles the samples are plasma-etched with a radio frequency oxygen plasma: this removes the used polymer. To form metallic nanoparticles, the oxygen plasma is followed by a hydrogen plasma. The arrangement of these nanoparticles can be studied using AFM or SEM. With in situ XPS the cleanliness and the chemical status of the nanoparticles can be studied. The particle size and the order of the nanoparticles are influenced by the loading ratio and dip-coating speed respectively. Also the polymer used is important for these parameters. The polymer used consists of a polystyrene (PS) and a poly-2-vinylpyridine (P2VP) block (figure 2). While the size of the PS-tails has an influence on interparticle distance, the size of the P2VP-heads influences the size of the nanoparticle.[26, 27]

As an example, figure 3 shows the morphology of $Fe_{48}Pt_{52}$ nanoparticle arrays on Silicon(Si)-substrates prepared by using the micellar approach. The SEM-images in figure 3 clearly show that the arrangement of the particles is equal before (figure 3b) and after heat treatment (annealing at 650°C for 45 min) (figure 3c) and no aggregates are formed during this process.[21, 22]

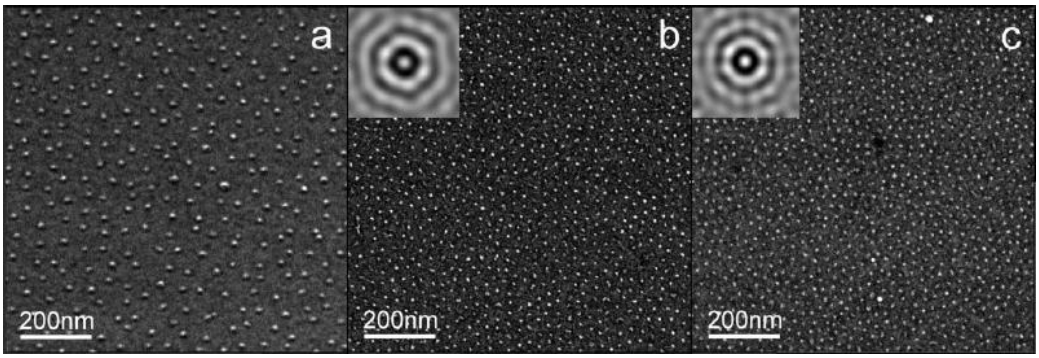

Figure 3: The morphology of $Fe_{48}Pt_{52}$ nanoparticle arrays on Si substrates prepared by using a micellar method. SEM images of (9.4 ± 1.1) nm particles (a) and (4.5 ± 1.3) nm particles (b), deposited by using a dip-coating process after the different plasma steps. Image (c) presents the ensemble shown in (b) after annealing to 650°C for 45 min . Obviously, the quality of the array was maintained during this process. Figure is from Ethirajan et al., Adv. Mater. 2007(19): 406-410.

1.2) Characterization techniques

1.2.1) Atomic Force Microscope (AFM)

The AFM is a powerful instrument for investigating both conducting and insulating surfaces. The AFM can image almost any type of surface, including polymers, ceramics, composites, glass, and biological samples. The AFM relies on the forces (Van der Waals force, dipole-dipole interaction, electrostatic forces, etcetera) between the extremely fine, sharp tip and the sample. The tip is attached to a cantilever which acts like a spring. The force (F) between the tip and the sample causes a deflection of the cantilever (X) (Hook's law[28]). These deflections are monitored by a photodiode and processed using imaging software. The resulting image is a topographical representation of the sample that was just scanned. Deflection of microns to 0.1 Å can be measured with the photodiode.[29-31]

During non-contact mode the tip stays 10 to 100 nm above the sample. When the tip scans across the surface, it will interact with it, and deflect according to the interaction. A feedback mechanism is employed to adjust the distance between sample and tip to maintain a constant force between them. The sample is often mounted on a piezoelectric element, which can move the sample in the *z* direction for maintaining a constant force, and the *x* and *y* directions for scanning the sample (figure 4A). During non-contact mode it is possible to use tapping mode, where the tip vibrates above the surface of the sample. The difference in attractive forces between sample and tip changes the vibration amplitude of the tip. By calculating the difference in drive amplitude and measured amplitude of the tip a phase image can be made with imaging software.[30]

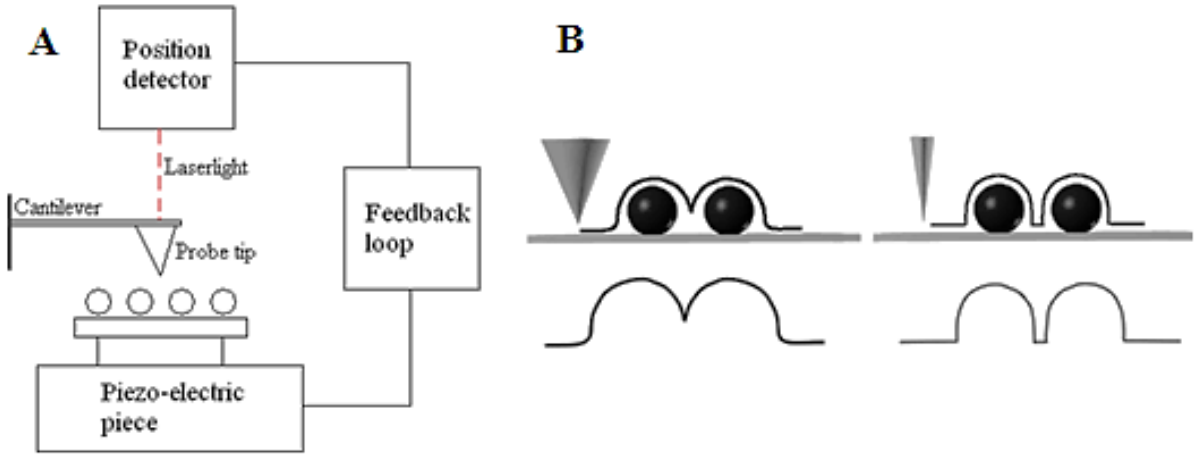

Figure 4: Atomic force microscopy. A: Block diagram of a AFM. B: Tip-broadening effect.

When sample and tip are separated in the order of Å, then the tip is in contact with the sample, here the ionic forces are more important. Contact mode allows a high resolution image of the surface to be formed. The resolution depends on the width of the tip, thinner tips give a better resolution. This is called the tip-broadening effect (figure 4B). It is important to note that in contact mode the sample can be damaged by the tip. When imaging soft polymers or soft biological material tapping mode is used[30], therefor in this work tapping mode was applied.

1.2.2) X-ray Photoelectron Spectroscopy (XPS)

XPS is a widely used technique to investigate the chemical composition of surfaces. XPS is a quantitative spectroscopic technique that measures the elemental composition, chemical state and electronic state of the elements that exist within a material. An x-ray spectrometer has several required components to perform a measurement (figure 5A). These include a vacuum chamber, an x-ray source (AlKα), a load lock, a detector and a system for processing the data. Ultrahigh vacuum of 10^{-9} Torr is needed to avoid collision of the x-rays with gas molecules and of gas molecules with the surface. The energy of the X-ray has to be sufficient to excite photoelectrons of all elements, but at the same time the natural linewidth of the x-ray transition should be narrow to obtain a high energy resolution. The use of a load lock reduces the time needed to reach the required vacuum level for measuring, because only a small chamber needs to be vented when introducing a sample. The different components of a XPS device were optimized to measure binding energy differences of 0.1 eV or even more accurate.[32, 33]

When a material is irradiated with a beam of X-rays the kinetic energy and number of electrons that escape from the surface are measured (figure 5B). The binding energy of the emitted electrons can be calculated by using equation 2.[33]

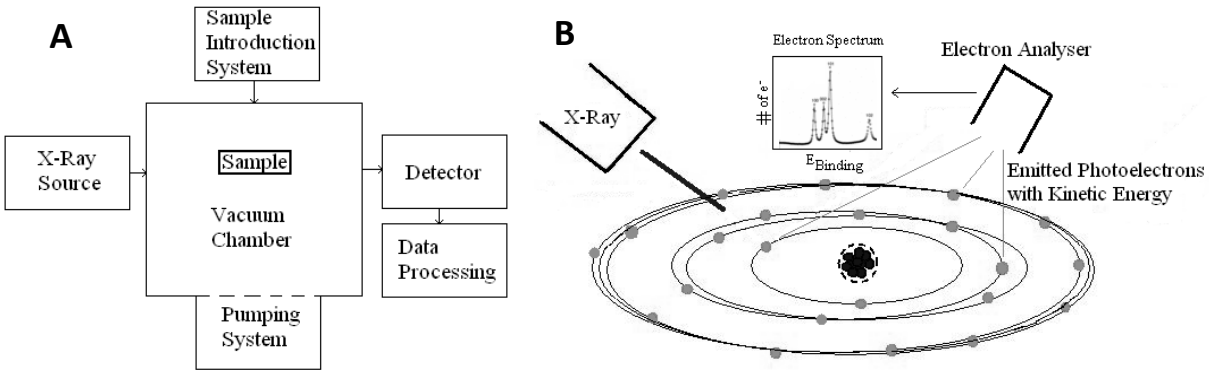

Figure 5: X-ray photoelectron spectroscopy. A: Block diagram of XPS. B: Schematic overview of the working principal of XPS.

$$E_{\text{binding}} = E_{\text{photon}} - (E_{\text{kinetic}} + \phi)$$

Equation 2: Calculation of binding energy. $E_{binding}$ is the binding energy of the electron, E_{photon} is the energy of the X-ray photons being used, $E_{kinetic}$ is the measured kinetic energy of the electrons and Φ is the work function of the spectrometer.

It is possible to directly identify each element that exists in or on the surface because each element produces a characteristic set of XPS peaks at defined binding energy values. These peaks correspond to the electron conformation of the electrons in the atoms (1s, 2s, 2p, 3s, etcetera). All of the deeper photo-emitted electrons are either recaptured or trapped in various excited states within the material. XPS cannot identify hydrogen and helium because these are very small atoms and electron emission does not take place easily. As electron density is dependent on the electronegativity of neighboring atoms information about the surrounding environment and its interference can be measured. The resulting shift in the XPS measurements is called chemical shift.[33]

1.2.3) Electrochemical Impedance Spectroscopy (EIS)

The concept of electrical resistance is well known, it is the ability of a circuit element to resist the flow of electrical current. A known definition of electrical resistance is defined by Ohm's law ($R = \frac{V}{I}$)[34]. This law has a limited use: it only applies to an ideal resistor or a resistor under direct current. An ideal resistor follows Ohm's law at any current (I) and voltage (V) levels. The ideal resistance (R) level is independent of frequency therefore alternating current (AC) and voltage signals are in phase with each other.

Many circuit elements have a more complex behavior where AC current and voltage signals are not in phase at certain frequencies. In these systems the ability of a circuit element to resist the flow of electrical current is called impedance (Z). Impedance can be measured by applying an AC potential to a cell and measuring the resulting AC current. In a pseudo-linear system, created by using a small excitation signal, the response to a sinusoidal potential will be a sinusoidal current at the same frequency but shifted in phase. This phase-shift makes impedance a complex quantity, consisting of a real and imaginary part. At certain frequencies the phase-shift will be more pronounced.[16, 35]

Impedance measurements are often analyzed by fitting the data to an equivalent electrical circuit model. Such an electrical circuit can contain resistors, capacitors and inductors. The formulas to calculate impedance of these electrical components are given in table 1. As can be seen in the table: the impedance of a resistor is not frequency dependent. The impedance of a capacitor and inductor on the other hand are frequency dependent. A basic equivalent electrical circuit for impedance measurements is the Randles cell (figure 6A).

Table 1: Impedance of components of an electrical circuit.

Component	**Z**
Resistor (R)	$Z=R$
Capacitor (C)	$Z=1/i\omega C$
Inductor (L)	$Z=i\omega L$

Impedance data can be presented with a Nyquist plot, the real part of impedance is plotted on the X-axis and the imaginary part on the Y-axis. Every point of the graph is the impedance at a certain frequency. The lower frequencies are found at the right side of the plot and the higher frequencies are found on the left side (figure 6B). Because a resistor is independent of the frequency it only has a real impedance component. It can be seen on the X-axis of the Nyquist plot that the semi-circle starts at 0.01 Ω, this is due to the solution resistance (R_s). The difference between the two points on the X-axis is due to the charge transfer resistance (R_{ct}). A capacitor only has an imaginary impedance component, which means that the current is phase-shifted 90 degrees (for a pure capacitor) with respect to the potential. From the frequency at this 90 degree phase shift the capacitance of the double layer can be calculated ($\omega = 1/RC$). If the phase shift does not reach 90 degrees then the highest phase shift is taken instead.

Data can also be presented with Bode plots. The phase or the logarithm of the impedance is plotted on the Y-axis and on the X-axis the logarithm of frequency is plotted (figure 6C). The R_s (higher frequencies) and the sum of R_s and R_{ct} (lower frequency range) can be read of the impedance bode plot. The phase angle does not reach 90 degrees as it would for a pure capacitive impedance. If the values for R_s and R_{ct} were more widely separated the phase would approach 90 degrees. A third option is to look at the impedance over time at a certain frequency.[16, 35]

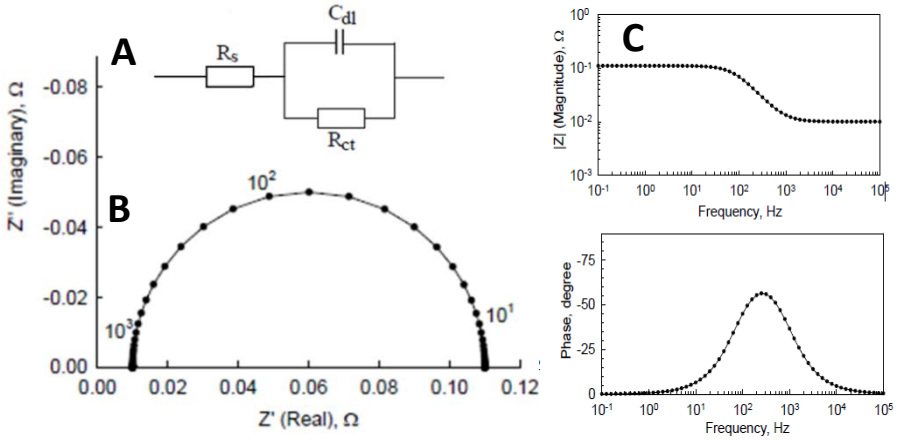

Figure 6: Different presentations of impedance data. A+B) The Nyquist plot is given for a Randles cell with a solution resistance (R_s) = 0.01 Ω, a charge transfer resistance (R_{ct}) = 0.1 Ω and the capacitance of the double layer (C_{dl}) = 0.02 F. Three frequencies are indicated in the Nyquist plot. C) Bode plots are given for the same Randles cell.

Impedance spectroscopy can be divided in to two main categories: EIS and not-EIS. Not-EIS applies to dielectric materials whose electrical characteristics involve dipolar rotation and to materials where electrical conduction predominates, for example single crystals and amorphous semiconductors, glasses and polymers. EIS involves measurements of systems in which ionic conduction predominates, as used during this research. EIS is therefore useful to study for example liquid electrolytes, ionically conducting glasses and polymers, fuel cells, corrosion, etcetera.[16, 35]

2) Experimental part

2.1) Materials and instrumentations used

The polymer, PS(32500)-*b*-P2VP(7800), was obhtained from Polymer Source (Dorval, Canada). $HAuCl_4$ was acquired from Sigma-Aldrich. The probe DNA with sequence 5'-HS-CGCATTCAGGAT-3' and the complementary (c)DNA with sequence 5'-ATCCTGAATGCG-3' were bought from Thermo Fisher Scientific (Ulm, Germany). Sodium hydroxide was acquired from Merck (Overijse, Belgium). Poly Chain Reaction (PCR)-buffer (contains 0.05 M KCl and 0.01 M tris-HCl with pH = 8.3 at room temperature (RT)) and Sodium dodecyl sulphate (SDS) were acquired from Roche (Belgium) and VWR International (Zaventem, Belgium), respectively. Phosphate buffered saline (PBS) (10x PBS contains 1.29 M NaCl, 0.05 M Na_2HPO_4*2 H_2O, 0.015 M KH_2PO_4 with pH = 7.2 at RT) and Sodium chloride sodium citrate (SSC) (20x SSC contains 3 M NaCl and 0.3 M $Na_3C_3H_5O(COO)_3$) were homemade. Hydrogen chloride (HCl), hydrogen peroxide (H_2O_2), ammonium hydroxide (NH4OH), acetone and isopropanol were purchased at VWR international (Leuven, Belgium). Demin water obtained from Arium 611DI or an Arium proVF (both from Sartorius, Germany) was used.

N-type Si-wafers (thickness 525 ± 15 µm, 111 orientation) highly doped with phosphorous (0.009 – 0.0111 Ωcm) were acquired from WaferNet Inc. (San Jose, California, United States of America). The impedance spectrometer with flow cell setup was built-up around an Analog Device AD5933. Etching device and dip-coating set-up were home built. XPS analyzer is from SPECS. The load lock and sample preparation chamber coupled to the XPS analyzer are custom built. Iviumstat and HP 4194A impedance/gain-phase analyzer were purchased at Ivium technologies (Eindhoven, The Netherlands) and at Hewlett Packard respectively. AFM images were made with a Digital Instruments Nanoscope IIIa of VEECO (Mannheim, Germany).

2.2) Optimizing substrate shape and dip-coating

To measure impedance with the home-built flow cell setup, square substrates with 10 mm sides are required. As dip-coating set up was optimized for samples with a width of 5 mm and a height of 10 mm, containers with appropriate dimensions were used to dip-coat the larger substrates.

2.3) Production of nanoparticles with the micellar approach

To optimize the different processes, polymer PS(32500)-*b*-P2VP(7800) was used to make size-selected nanoparticles. In a first step a micellar solution was made. The container (to hold the solution) and lid, tweezers, a magnet and a knife were cleaned with toluene and dried with nitrogen. There were several solutions made, all consisting of 5 mg polymer/ ml toluene. The

polymer was dissolved to form micelles by magnetically stirring the solution for three days. These micelles were loaded with a metallic salt, $HAuCl_4$. Before adding $HAuCl_4$ to the solution, the spatula to handle the salt was cleaned with isopropanol and dried with nitrogen. The amount of salt added, the loading ratio and other specifications for each solution is given in table 2. The salt-loaded solutions were magnetically stirred for seven days. When the salt-loaded micelles reached equilibrium they were dip-coated on a Si-, tantalum pentoxide (Ta_2O_5) or diamond substrate.

Table 2: Overview of the salt-loaded solutions made.

Solution	Polymer Amount (mg)	Molecular weight PS (U)	Molecular weight P2VP (U)	Loading ratio	HAuCl4 calculated (mg)	Amount of HAuCl4 added (mg)
404	24.6	32500	7800	0.50	7.7	8.0
412	25.5	32500	7800	0.50	8.0	8.1
418	25.4	32500	7800	0.50	8.0	7.9
434	25.1	32500	7800	0.50	7.9	8.0
473	25.1	32500	7800	0.50	7.9	7.9
474	25.0	32500	7800	0.50	7.8	7.7
518	25.2	32500	7800	0.50	7.9	7.9

The Si-substrates were cleaned using different procedures. The first procedure of cleaning consisted of the RCA-cleaning protocol[36-38]. It was used for samples after cutting the Si-wafer. The complete RCA-cleaning protocol consisting of two parts is given in supplemental part 1 and 2. In the first part[37] organic residue was removed from the Si-wafer. A solution of clean water (325 ml) and NH_4OH (65 ml) was heated up to 75 °C. 65 ml H_2O_2 was added to the solution. After 1 to 2 minutes when it started to bubble vigorously, the solution was ready for use. After soaking the Si-substrate in the solution for 15 min, the substrate was rinsed with flowing water. In the following part[38] metallic ions were removed from the Si-substrate. HCl (50 ml) was carefully added to 300 ml of clean water and heated up to 75 °C. A few minutes after adding 50 ml H_2O_2 to the solution, it started to bubble vigorously. This bubbling indicated that the solution was ready for use. The Si-substrate was soaked in the solution for 10 min and rinsed with clean water. The substrate was dried with nitrogen.

However, the above described cleaning procedure was considered aggressive for the substrate and therefore all further cleaning was performed with the following cleaning procedure: The cleaning procedure consisted of consecutive steps of washing in acetone, isopropanol and water. The Si-substrates were ultrasonicated 10 min in acetone and 10 min in isopropanol. After repeating this step two times, the substrates were cleaned for 5 min by ultrasonification followed by cleaning in fresh hot water for 5 min. This step was repeated three times. On the Si-substrates PMMA was spincoated to ensure that dust and other contaminants did not attach to the surface during cutting and storage. Before dip-coating this cleaning protocol was used again to remove the PMMA-layer. This cleaning protocol was also used for the Ta_2O_5- and diamond substrates, these substrates where not treated with PMMA for cutting and storage.

When dip-coating, the tweezers, screwdriver, rod of dip-coating machine and substrate were cleaned with toluene and dried with nitrogen. The substrate was mounted into the dip-coating device and the solutions were filtered before dip-coating, with an assembly of three filters (1 µm, 0.45 µm and 0.2 µm pores). Salt loaded micelles created from polymer PS(32500)-*b*-P2VP(7800) were dip-coated with a speed of 6 mm/min. The samples with the micelles were characterized using AFM. The dip-coated samples were then plasma-etched with a radio frequency oxygen plasma (30 min, room temperature (RT)) to remove the polymer coating. The samples were then treated with hydrogen plasma (30 min, 250 °C) to reduce the gold oxide to gold metal and again characterized by AFM.

2.4) Functionalization of gold nanoparticles with DNA

In a first step, probe DNA was attached to the gold nanoparticles. The substrate with gold nanoparticles was soaked in 1x PBS to wet the surface. Before transferring the sample to a Petri dish the sample was held sideways so that the PBS could drop off. Next to the sample some water was added in the Petri dish to avoid evaporation of the DNA-solution. The probe DNA (10 pmol/µl, 30 µl) was pipetted on the sample. The Petri dish was closed and was placed for 15 hours in the incubator at 37 °C. The unbound probe DNA was washed off with 1x PBS and the sample was stored inside 1x PBS.

In a next step complementary (c)DNA was hybridized with the probe DNA attached to the gold nanoparticles. 6 µl of cDNA (100 pmol/µl) was added to 14 µl of 1x PCR-buffer to make a hybridization mixture. The sample was transferred from 1x PBS to a Petri dish; during the transfer the sample was held sideways to allow the PBS to drop off. The hybridization mixture (20 µl) was then transferred to the sample. Some water was added to the Petri dish next to the sample. The sample was incubated for 2 hours at 37 °C. Then the sample was held sideways to remove the hybridization mixture and the sample went through a rinsing cycle. First it was rinsed with 2x SSC/ 0.5% SDS (30 min, RT), then two times with 0.2x SSC (5 min, RT) followed by a final rinsing step in 1x PBS (0.5 min, RT). Between each rinsing step most of the solvent was removed from the surface. The samples were stored inside 1x PBS at 4 °C. For the repeatability measurements the same hybridization procedure was used after each EIS cycle.

2.5) Characterization of substrate and particles

2.5.1) Atomic Force Microscope (AFM)

The quality of the ordering of the micelles was studied with the AFM before etching. After etching the nanoparticles were again characterized with AFM. Parameters such as hexagonal order, particles/cm^2, size distribution and interparticle spacing were taken into account. All these parameters have an influence on the quality of the biosensor setup and the repeatability of the measurements with this biosensor.

2.5.2) X-ray Photoelectron Spectroscopy (XPS)

After etching the cleanliness of the surface was measured with in situ XPS using a surface scan (sweeping from 0 eV to 1400 eV). Only clean samples, without contamination where used for further measurements. After etching in the plasma traces of copper, molybdenum, and sodium were observed in the survey scan on the sample. While copper and molybdenum signals were originating from the etching device, the sodium signal was from sample handling.

To measure the amount and chemical state of the gold nanoparticles a scan was done for binding energies ranging from 80 eV to 94 eV. In this region Au 4f peaks are located. Also a scan was done for binding energies ranging from 98 eV to 108 eV (contains Si 2p peaks); the latter was done to investigate the amount and the chemical state of Si and SiO. The state of the gold nanoparticles and of the substrate were studied after each step.

2.5.3) Electrochemical Impedance Spectroscopy (EIS)

IMO provides several setups to measure impedance. The setup shown in figure 7 was used for most of the measurements; this system was well characterized by Van Grinsven et al.[39] Figure 7 gives the schematic overview of the electrochemical impedance spectrometer with the home-built flow cell setup. In this setup, it is possible to add different fluids to the cell using a pumping system and a three way valve. The temperature inside the fluid and the copper can be monitored and controlled with a thermocouple.[5, 39] This impedance spectrometer will in the further text be referred to as the home-built flow cell setup. With the home-built flow cell setup it was possible to connect measuring chambers in which one, two or four samples could be measured at a given time. In this work only one sample was measured at a time.

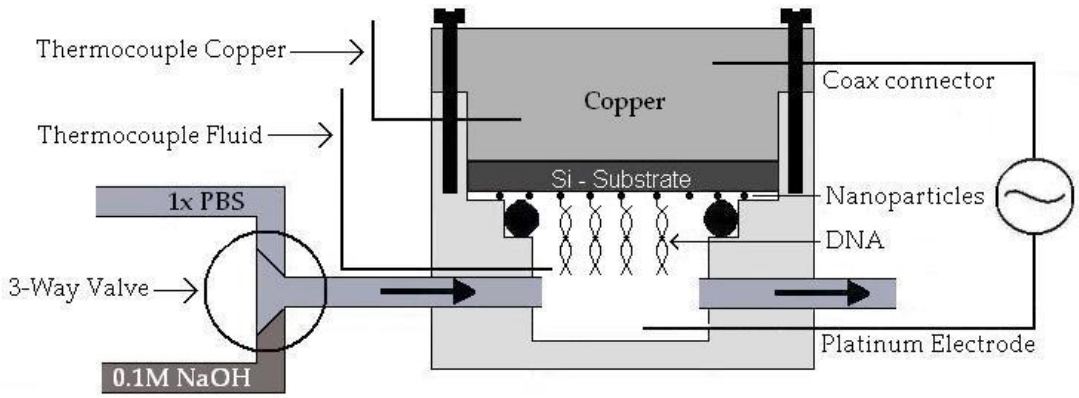

Figure 7: Schematic representation of a home-built flow cell setup as designed by Van Grinsven B. et al., Physica Status Solidi, 2010. 207(4): 919-923.

To study the substrates (Si, Ta_2O_5 and diamond), the gold nanoparticles and their DNA-binding behavior, EIS was used. The pumps of the home-built flow cell setup were programmed so that the gold nanoparticles were measured before, during and after the denaturation of the DNA (figure 8). The measurements were started by pumping 0.1x PBS (12 min) inside the measuring cell. This way it was possible to detect air early in the

measurement, as an air bubble inside the measuring cell will work as an insulator and impedance levels will exceed 100 kΩ. After this test, the hybridized sample was measured inside a 0.1x PBS environment for 35 min. After that NaOH (12 min) was pumped into the measuring cell. The NaOH resided for an extra 28 min inside the measuring cell to ensure complete denaturation of the dsDNA. The cell was rinsed with 0.1x PBS for 12 min; this step washed the NaOH and the denatured DNA away. As a next step NaOH (12 min) was pumped into the measuring cell. The NaOH resided for an extra 28 min inside the measuring cell. As a final step the cell was rinsed with 0.1x PBS (12 min). The second NaOH step was needed to discern between the impedance change caused by the changing the solvent from PBS to NaOH and that caused by the denaturation of DNA. The temperature of the copper electrode was kept constant at 37 °C during the entire measurement. The pumping speed (0.125 ml/min - 0.25 ml/min) of the solvents and the concentration of NaOH (0.1 M or 0.01 M) was changed during the measurements to optimize the biosensor setup. The reference samples: bare substrate, sample with gold nanoparticles and sample with gold nanoparticles and probe DNA, went through the same cycle.

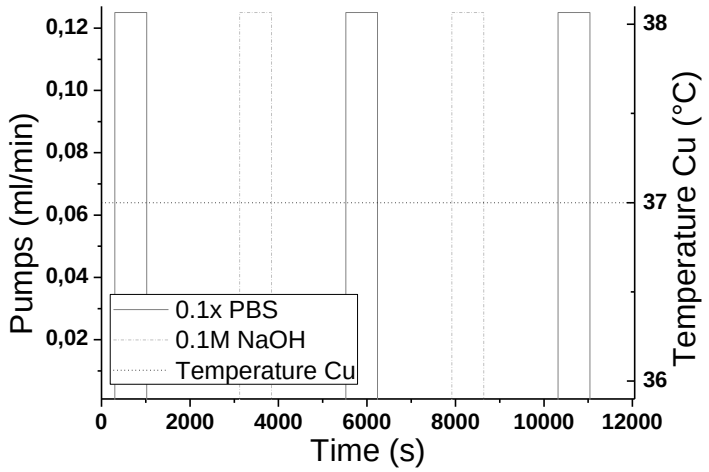

Figure 8: Graphical representation of the pumping cycle used in an EIS measurement to discern the sensitivity of the nanoparticles used, for all three substrates. Here a pumping speed of 0.125 ml/min was used.

Impedance measurements were also used to measure the temperature dependence of the bare Si- and Ta_2O_5-substrate. During this EIS measurement the temperature of the copper electrode was changed from 35 °C to 85 °C and back at a rate of 1 degree per minute (figure 9). This temperature change also influences the temperature of the fluid inside the measuring cell. Because both temperatures were monitored it was possible to calculate the temperature dependence of the substrates.

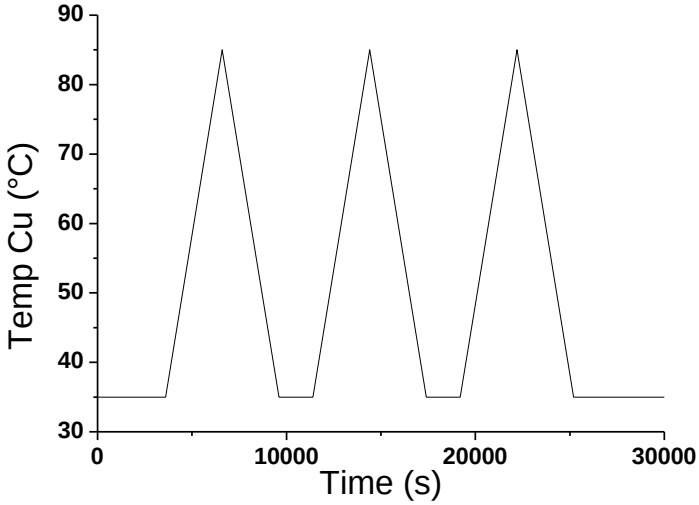

Figure 9: Graphical representation of the temperature cycle used in an EIS measurement to discern the temperature dependence of the Si- and Ta_2O_5-substrate.

The home-built flow cell setup measured the samples at 31 frequencies ranging from 100 Hz to 100 kHz. The Iviumstat device was used to measure the impedance at lower frequencies (0.15 Hz to 1 kHz). The HP 4194A impedance/gain-phase analyzer was used to measure impedance at frequencies ranging from 100 Hz to 1 MHz. The measurements of the Iviumstat and of the HP 4194A impedance/gain-phase analyzer were used to make Nyquist plots over a broad frequency range.

3) Results and discussion

3.1) Optimized substrate shape and dip-coating

There was a critical need to think about the design and dimensions of the substrate used, as the requirements for the sample holder in the etcher and the home-built flow cell setup were significantly different. In figure 10 the dimensions of the sample holder for etching (A) and the O-ring for the home-built flow cell setup (B) are shown. The sample had to be smaller than 5.5 mm at one corner so that it could be fixed in the sample holder for etching and at the same time the sample should be bigger than the O-ring with an outer diameter of 8 mm. To achieve this, the substrate was cut into 9 mm^2 and then three corners were removed so that a tear shaped sample was created (figure 10C). Figure 10D shows the overlay of the 3 parts (holder, sample and O-ring); it can be seen that by cutting the substrate in this way, it is usable for plasma etching and EIS.

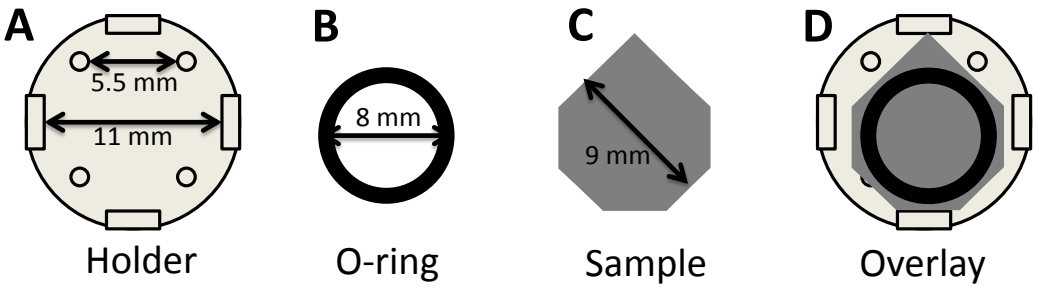

Figure 10: Optimization of shape and size of Si-substrate. A) Dimensions of the sample holder for etching. B) Dimensions of the O-ring for the impedance device. C) New design and dimensions for samples. D) Overlay of different components to show the compatibility.

As the samples are dip-coated from a toluene based solution, it was necessary to consider the drying speed of toluene, because this affects the arrangements of the micelles. Therefore several containers with different dimensions of neck and caps were tried out. Figure 11 shows AFM images of the samples dip-coated with a non-optimized bottle; it can be seen that micelles with no hexagonal order was obtained. The hexagonal order can be measured with the 2D autocorrelation graph (top right corner of figure 11). It can be seen in figure 11 that the micelles were closely packed and there were regions with less micelles. More AFM images for non-optimized containers are given in supplemental part 3.

As shown in figure 12, a wide-neck bottle (B) was finally used for dip-coating. For comparison, the standard bottle (A) used for the dip-coating of the 5 x 10 mm samples is also shown in figure 12. When characterizing the samples with AFM, it was seen that an high hexagonal arrangement of the micelles was obtained (figure 13).

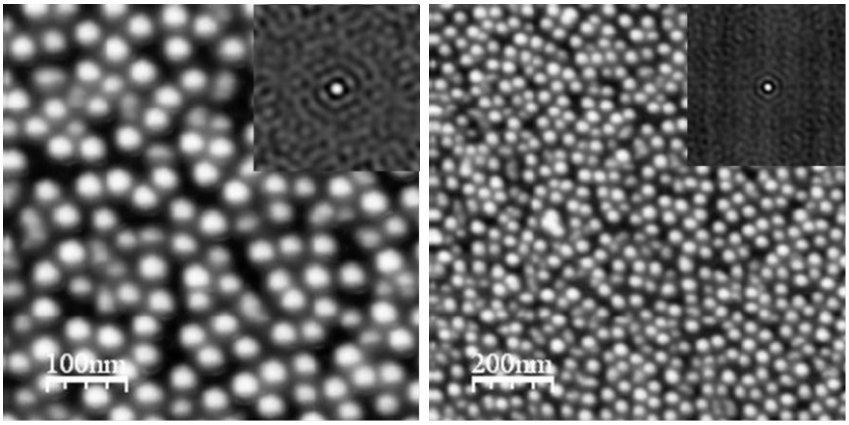

Figure 11: AFM images in different magnifications showing the arrangement of micelles (from solution 404) dip-coated on a Si-substrate from a non-optimized bottle.

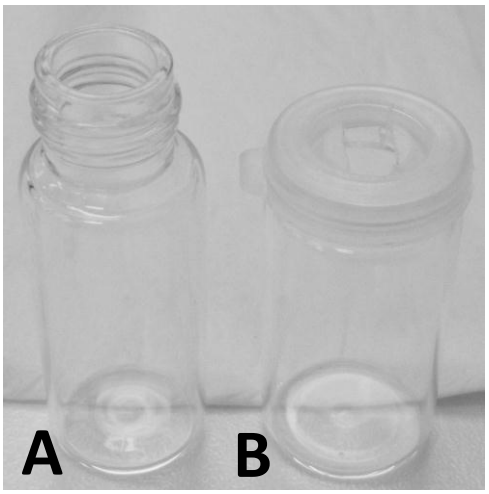

Figure 12: Comparison of the standard bottle used for dip-coating and the bottle used for the larger substrates. A) Standard bottle used for dip-coating for samples of 5 mm by 10 mm. B) Bottle used for dip-coating the larger samples.

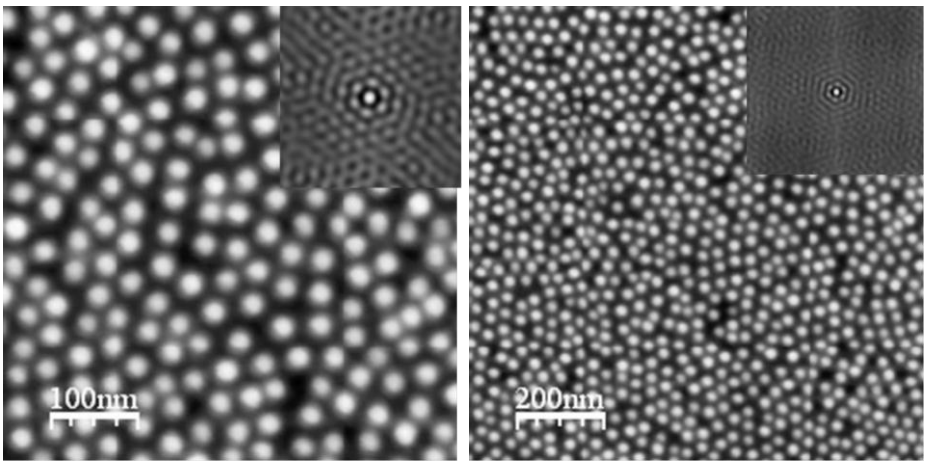

Figure 13: AFM images in different magnifications showing the arrangement of micelles (from solution 473) dip-coated on a Si-substrate from the optimized wide necked bottle and cap.

3.2) Characterization of gold nanoparticles with AFM

AFM was used to assess the quality of the micelles and of the nanoparticles. To guarantee the reproducibility of an EIS measurement it is important that there is a high hexagonal order of the gold nanoparticles, a fixed interparticle distance between them and a small size distribution of the particles. These parameters can be determined from the AFM images by using Gwyddion software.[40] As the amount of particles in the measuring area has to be comparable for each sample and therefore the amount of bound probe DNA, it is very important that the before mentioned conditions are fulfilled. Figure 14 shows micelles and gold nanoparticles on a substrate after etching with O- and H-plasma. From the figure it is evident that the high hexagonal order is maintained after etching.

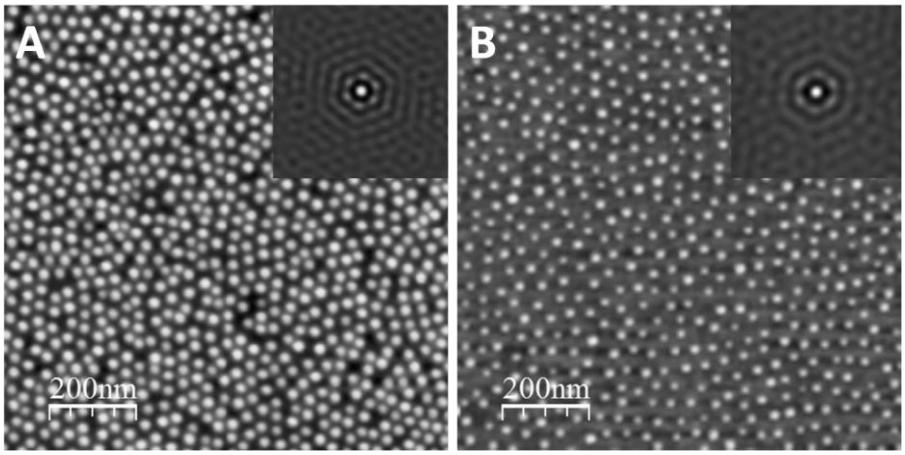

Figure 14: AFM image of nanostructures (A) micelles after dip-coating and (B) gold nanoparticles after etching on the substrate prepared by the micellar approach from solution 473.

Figure 15 A and B show gold nanoparticles on a Si- and Ta_2O_5-substrate, respectively. As Ta_2O_5-substrate (figure 15, B) has a higher roughness (Rms = 1.167 nm) than the Si-substrate (Rms = 0.147 nm; figure 15, A) the particles on the Ta_2O_5 appear smaller but measurements show that this is not the case (figure 16). In supplemental part 4 more AFM measurements of etched samples are given.

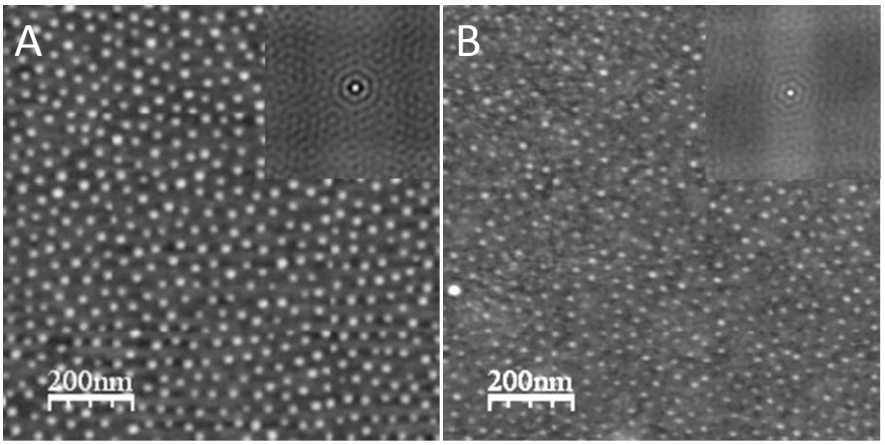

Figure 15: The morphology of gold nanoparticles prepared by the micellar approach. A) Nanoparticles on a Si-substrate (from solution 473). B) Micelles on a Ta_2O_5-substrate (from solution 474).

Figure 16 shows the particle size distribution for the same samples as in figure 15. The nanoparticles ordered on the Si-substrate have an average particle size of 2.6 nm, with a full width half maximum (FWHM) of 0.31 nm. The gold nanoparticles on the Ta_2O_5-substrate have an average particle size of 2.7 nm with a FWHM of 0.59 nm.

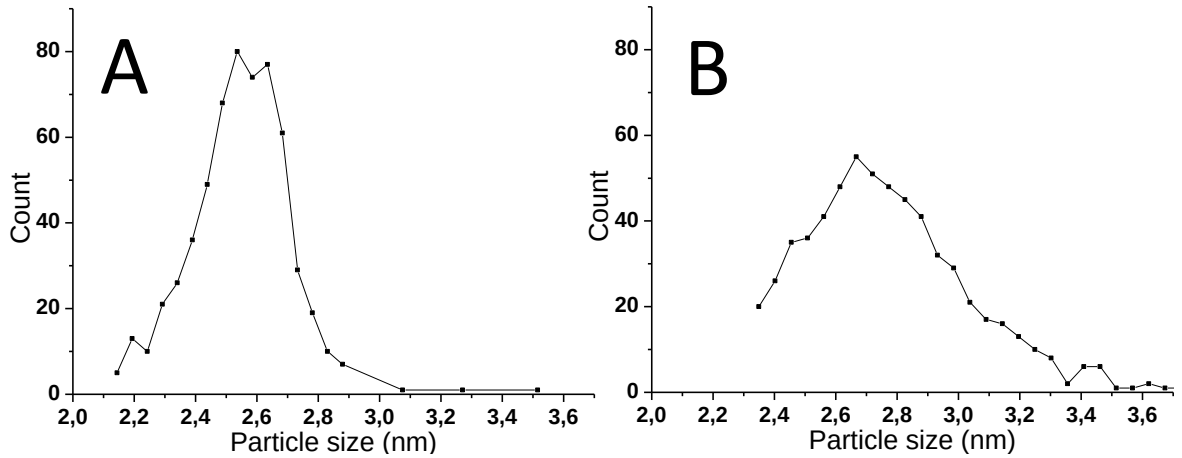

Figure 16: Particle size distribution of the samples shown in figure 15. A) Particles on a Si-substrate made from solution 473. B) Particles on a Ta_2O_5-substrate made from solution 474.

The amount of bound probe DNA is important for the sensitivity of the biosensor. The bound probe DNA can be estimated from the amount of gold nanoparticles per square centimeter. The Gwyddion software counted 594 particles for 1 μm^2 for the micellar solution dip-coated on Si (figure 15, A). Because of the high hexagonal order it can be estimated that 1 cm^2 contains about $6x10^{10}$ gold nanoparticles with an average interparticle distance of 43 nm. With the software 616 particles where counted for 1 μm^2 on the Ta_2O_5-substrate (figure 15, B). Therefore it can be estimated that 1 cm^2 contains about $6x10^{10}$ gold nanoparticles with an average interparticle distance of 38 nm. If it is assumed that each particle only binds one probe DNA strand then the surface will contain 10^{10} strands, which is slightly lower than the reported density of 10^{12} strands for the fatty acid technique on diamond[5, 41].

Due to the higher roughness of the Ta_2O_5-substrate, AFM characterization was also made after functionalization of the nanoparticles with DNA to investigate if the gold nanoparticles were accessible for binding. Figure 17 A and C show an AFM-image of a Ta_2O_5-sample before and after attachment of probe DNA, respectively. As it can be seen here, there is a clear difference before and after attachment of DNA. The phase image (figure 17, D) shows that the nanoparticles are indeed larger after functionalization step. Thereby confirming the hypothesis that the gold nanoparticles are indeed available for functionalization, and the probe DNA is indeed bound to the gold nanoparticle after a tedious multistep washing procedure.

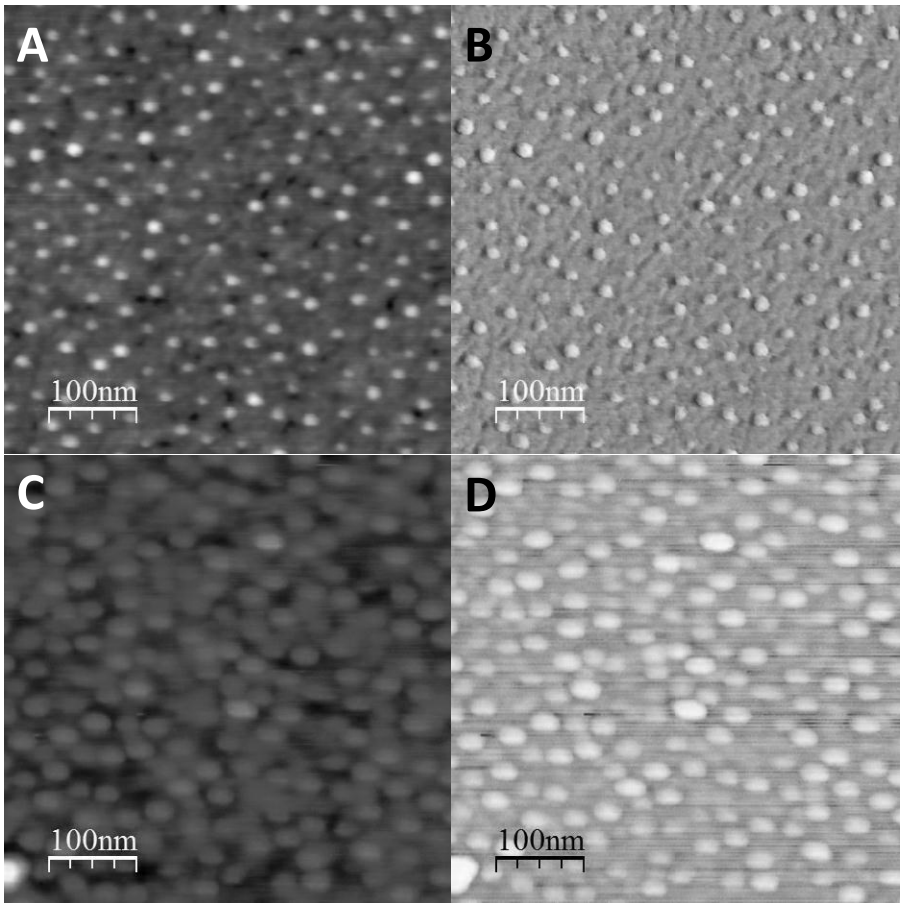

Figure 17: AFM-images of a Ta_2O_5- substrate with Au nanoparticles before (A & B) and after functionalization with dsDNA (C & D). The sample was made with solution 474. A and C are the height images before and after functionalization respectively, where B and D are the respective phase images.

Due to a limited time, available diamond substrates with a high roughness (Rms = 11.811 nm) were used as a substrate. Therefore the hexagonal order could not be guaranteed for these samples. Figure 18 shows the height and phase image of gold loaded micelles dip-coated on a diamond substrate. As the roughness of the substrate is quite high, it difficult to image the micelles with the reasonable resolution.

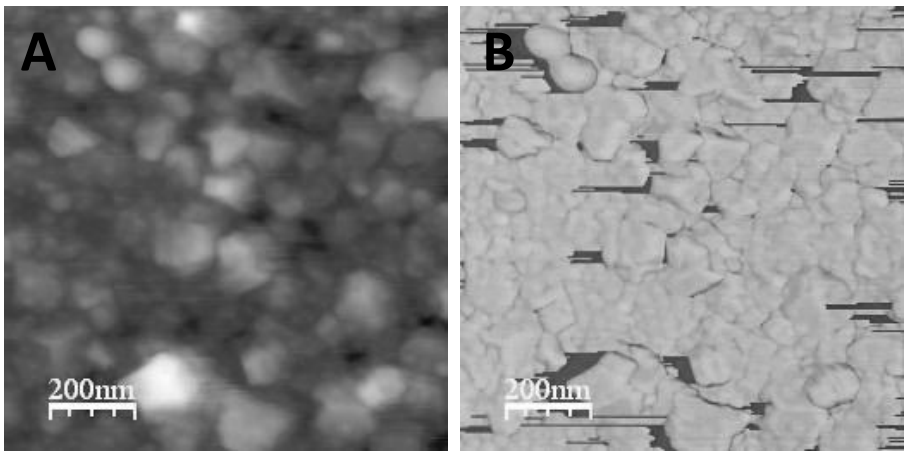

Figure 18: AFM-images showing micelles dip-coated (from solution 518) on a diamond substrate. A) Height image. B) Phase image.

3.3) Cleanliness of samples

The presence of contaminants can influence EIS measurements, therefore only clean samples were used for measurements. The cleanliness of each sample was measured with XPS directly after etching. The expected peaks for a clean substrate are that of the gold nanoparticles, the substrate itself (Si, Ta or carbon), oxygen, nitrogen and carbon. Figure 19 shows a in situ survey scan with XPS of a clean and contaminated Si-sample. The XPS scan of the clean sample show the expected peaks, but the curve for the contaminated sample also shows peaks for molybdenum and copper. The molybdenum is transferred from the sample holder and the copper is coming from the electrode for plasma etching. Other possible contaminants are sodium and chloride from handling.

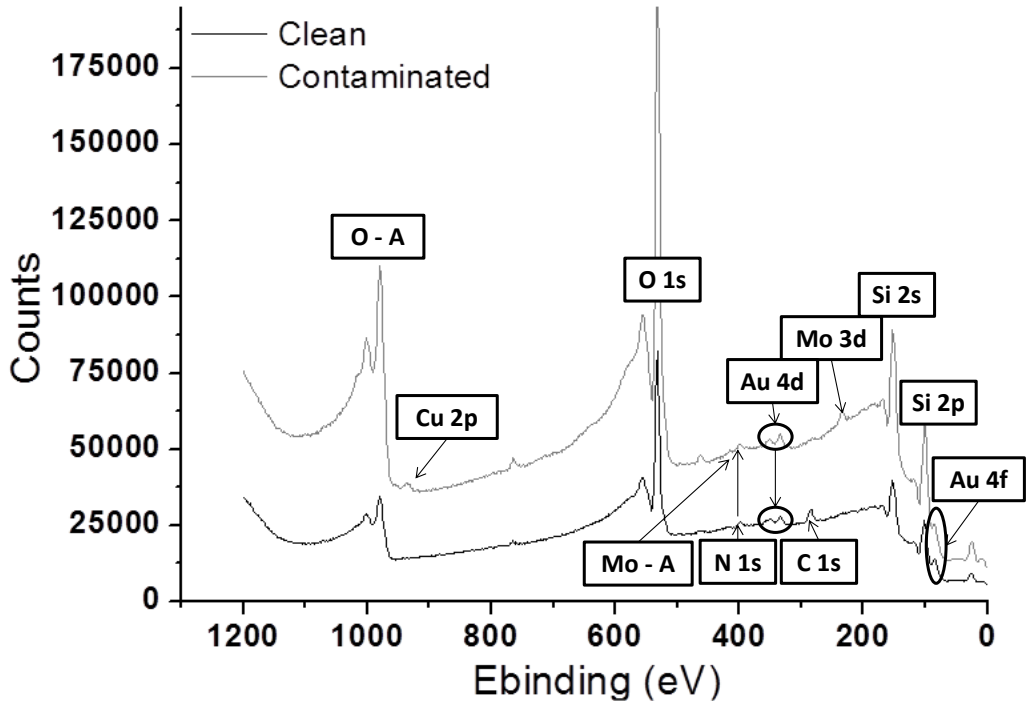

Figure 19: Surface scan with XPS of a clean and contaminated sample.

3.4) Temperature dependence of substrates

The temperature dependence of a substrate is very important for EIS measurements since the impedance is highly dependent on temperature. For each substrate the dissipated power, the thermal resistance (R_{th}) and the temperature difference between the temperature of the copper (connected to the substrate with silver paste) and the PBS (T_{Cu} - T_{PBS}) was calculated from the data collected during the measurement (figure 9, in experimental part 2.5.3). For the calculation of the power and R_{th} only the heating-up cycle is considered. Therefore each measurement is divided into two to three ramps. The dissipated power of the substrates is proportional to the square of the voltage applied to a resistor to heat up the copper, and inversely proportional to the resistor (22.2 Ω). The thermal resistance is a measure for T_{Cu} - T_{PBS} for each watt of dissipated power.

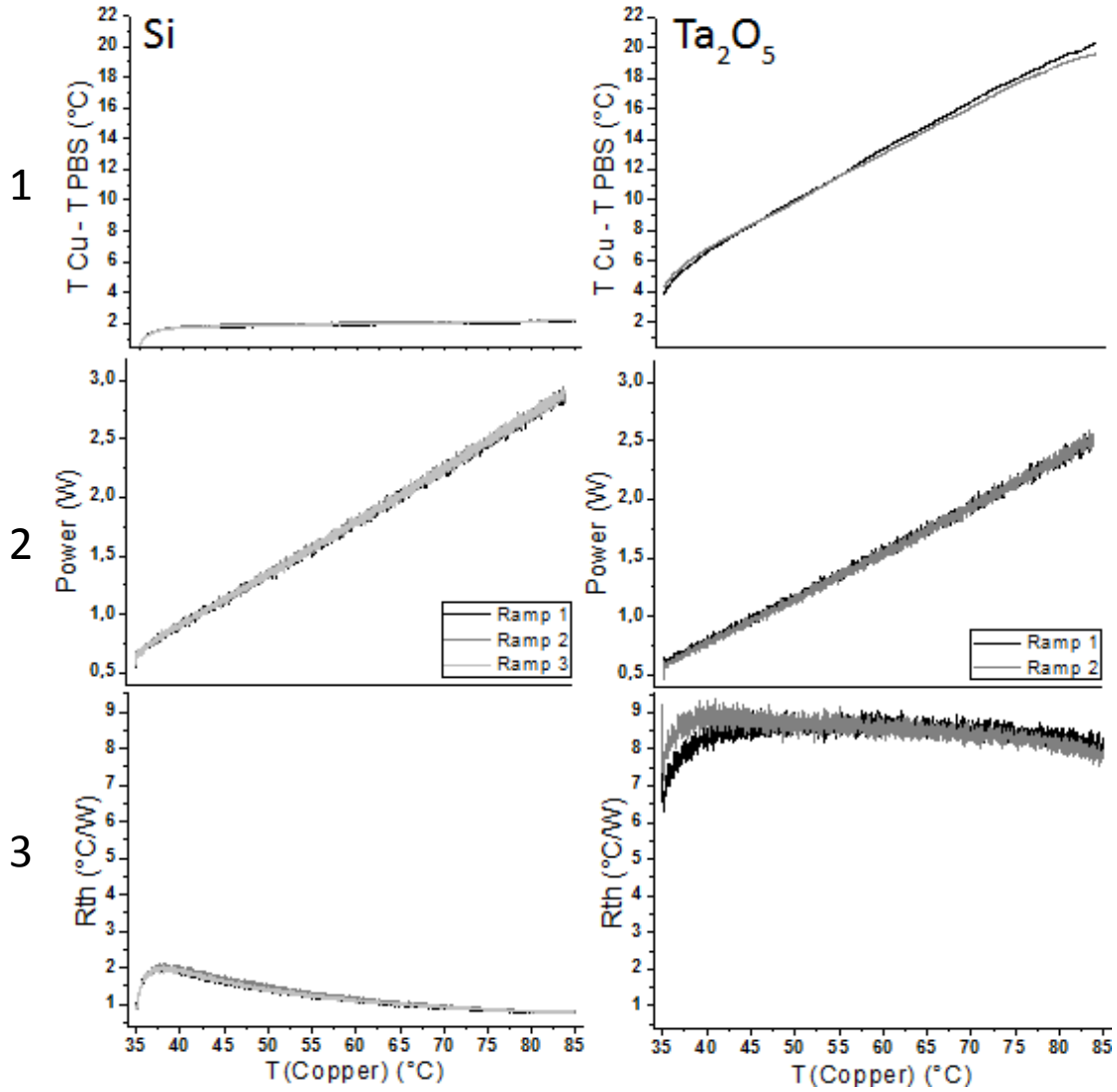

Figure 20: Temperature dependence of Si-substrates (left column) and Ta_2O_5-substrates (right column).

In figure 20 graph 1, it can be seen that T_{Cu} - T_{PBS} increases linearly with the temperature increase of the copper for both bare Si- and Ta_2O_5-substrates. The temperature difference between the copper and the PBS is rather small for a Si-substrate as compared to Ta_2O_5, as the thermal conductivity of Si is higher than that of the Ta_2O_5-substrates. The increase in temperature difference between the copper and the PBS inside the flow cell with the temperature increase of copper indicates that the PBS cannot follow the temperature rise in the copper. This also explains why the dissipated power rises with increasing T(copper) (figure 20, graph 2); a higher voltage is needed to achieve a higher copper temperature. The thermal resistance over the temperature of the copper is considered stable for both the substrates (figure 20, graph 3). The thermal stability of the substrates does not change when the copper is heated up to 85°C. As the temperature dependence does not change over time: ramp 1 is the same as ramp 2 and ramp 3.

3.5) Typical denaturation cycle

All EIS measurements shown in the following Results and Discussion part were performed at a pumping speed of 0.125 ml/min. The measurements at 0.25 ml/min gave unexpected results, three of these measurements are given in Supplemental part 5.

Not only the thermal stability is of importance but also the chemical stability of the substrate needs to be taken into account. It is very important that when denaturing with NaOH, only the dsDNA is affected and not the substrate nor the gold nanoparticles. This can be well understood from figure 21, where the complete denaturation cycle is presented for the individual elements (bare substrate, substrate with nanoparticles, gold particles functionalized with probe DNA and gold nanoparticles functionalized with probe DNA and hybridized with cDNA).

In general, the steps shown in figure 21 represents a typical denaturation cycle during an EIS measurement that was performed during this work. The PBS-levels (number 1, 5 and 9) of the reference samples are stable throughout the measurements. For the measurement where the sample contained cDNA the 5th and 9th level are equal to each other but lower than the impedance during stabilization period 1. This confirms the results presented by Van Grinsven et al.[5] on diamond samples.

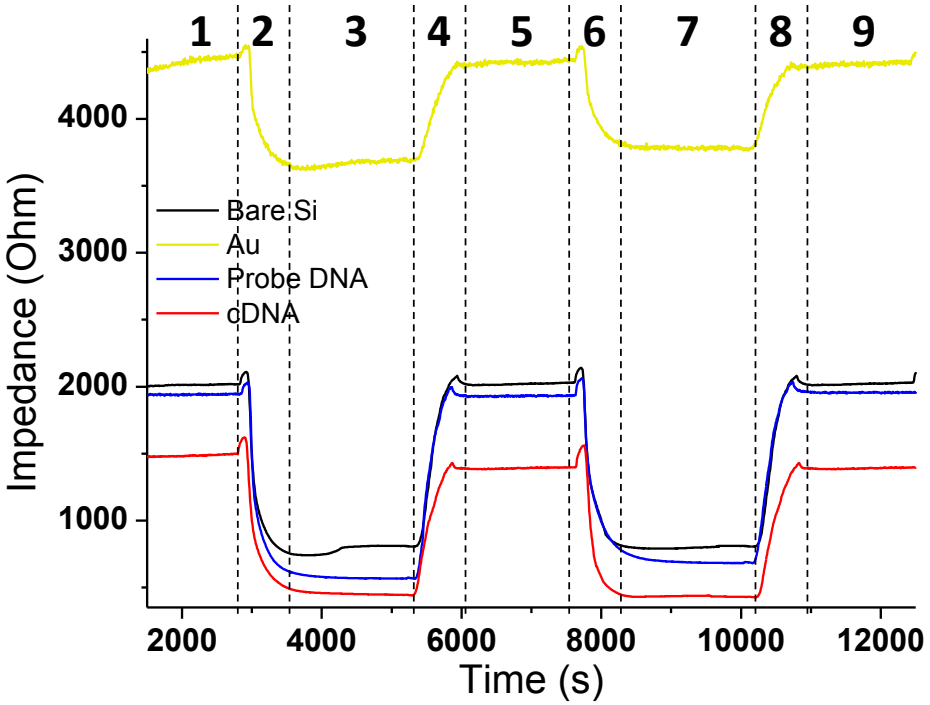

Figure 21: EIS measurement on different components in a typical denaturation experiment. Si-sample made with micellar approach from solution 434.

A typical denaturation cycle consists of stabilization periods and pumping periods, which divides the curves into nine steps. In the first step, the sample is stabilized inside PBS (1). After which NaOH is pumped into the cell (2) to denature the dsDNA followed by

stabilization in the NaOH (3). To remove the NaOH and the denatured DNA, PBS is pumped into the flow cell again (4). After a stabilization time in PBS (5), NaOH is pumped in to the cell (6) to measure the effect of NaOH alone. After stabilization in the NaOH (7), PBS is pumped into the flow cell (8) to check if the NaOH has completed the denaturation during the first NaOH-pumping step. As a final step, the sample is stabilized in the PBS (9). All the curves shown in figure 19 are at a frequency of 2511 Hz. The chosen frequency for the curves is the frequency where the phase difference is the biggest, which is selected after a frequency sweep. This frequency corresponds to the denaturation of DNA.

The first step at figure 21 represents the stabilization in a 0.1x PBS environment. It can be seen that after 1500 seconds the curves were stable for each element. The 2^{nd} and 6^{th} steps represent the pumping of NaOH (here 0.1 M) inside the measuring cell. Because of a sudden temperature drop during pumping the impedance first rises before dropping due to the ionic strength of NaOH and the denaturation of DNA (if cDNA is present). Steps 3 and 7 show the stabilization in the NaOH environment. It can be seen that stabilization occurs within minutes. During steps 4 and 8, 0.1x PBS was again pumped into the measuring cell; also here the impedance overshoots due to the drop in temperature during pumping. In the figure it can be seen that this impedance level of step 9 is the same as that of step 5, which means that all DNA is denatured during the first pumping step of NaOH (2) and during stabilization within NaOH (3). It can clearly be seen that in step 5 the impedance is lower after denaturation (cDNA), as compared to the other elements where the impedance goes to the same level as in step 1. The difference between the impedance level at stabilization step 5 (after denaturation) and 1 (before denaturation) is called the effect size. This effect size is therefore a measure for the amount of nanoparticles present for functionalization and the amount of denatured DNA.

3.6) Thermal resistance (R_{th})

For each measurement another interesting feature was seen during impedance measurements, because temperature was also monitored; the thermal resistance (Rth) before and after denaturation has a different level (figure 22).

In figure 22 the impedance measurement of sample A and B are shown in graph 1. These measurements have an effect size of 6.9% and 7.4%, respectively. The temperature of the fluid drops a few degrees during pumping (graph 2). In graph 2 it can also be seen that for both samples the temperature of the fluid changes during denaturation as indicated by arrows. One would expect that this drop in temperature might be due to a possible drop in the copper temperature. However, as can be seen in the same graph, the temperature of copper is constant over time. Also the power to heat-up the system does not change significantly (graph 3). Therefore, at this point, the only possible explanation for the temperature difference between copper and the fluid could be the change in R_{th}. This is evident from the bottom graphs (graph 4) of figure 22, where it clearly can be seen that after denaturation the R_{th} is higher than before performing denaturation. This is an interesting feature, currently being studied on diamond-based biosensors by Van Grinsven et al.

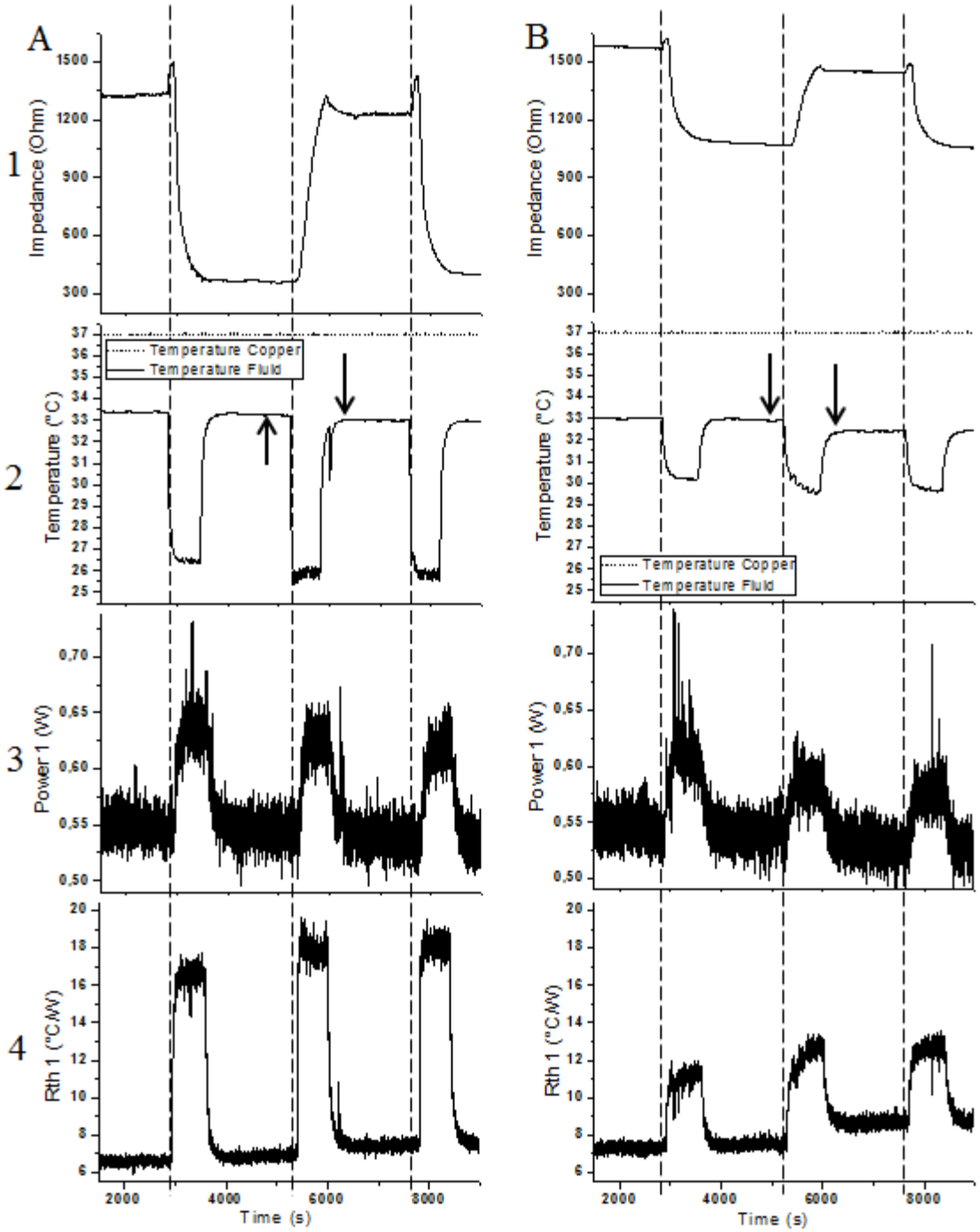

Figure 22: Impedance measurements (2511 Hz) and temperature dependence of two different Si-samples (A & B). Both samples were prepared from solution 412.

3.7) Repeatability of measurements

The consistency of EIS measurements on different samples as well as the reusability of the sensor surface is very important in order to guarantee a reliable biosensor. EIS measurements of the denaturation cycle on three different samples are presented in figure 23; for each sample the cycle was measured five times. All the samples were dip-coated from the solution 412. In general the effect size of all the 15 measurements was 5.6% ± 1.25%, which is a

significantly higher effect size than the average effect size of 3.4% ± 1.1% measured by Van Grinsven et al.[5].

As can be seen in figure 23, there was significant difference in the measured EIS cycles between different samples and also between different measurements of one sample. A possible reason that can explain small differences in impedance levels between the samples and between measurements of one sample, is the silver paste to attach the sample on the copper contact. If the silver paste-layer is not spread out correctly between the copper contact and the sample, voids filled with air can be formed between them. The impedance can then be higher, as air is not a good conductor. Also if the thickness of the silver paste is not the same for all measurements, small differences in impedance can be expected. Another possible reason for measuring impedance differences between samples is that each sample is unique, there each sample is made manually. Because these differences in impedance are small and only influence absolute impedance levels and not the difference between the state before (figure 21, step 1) and after denaturation (figure 21, step 5), these factors can be neglected.

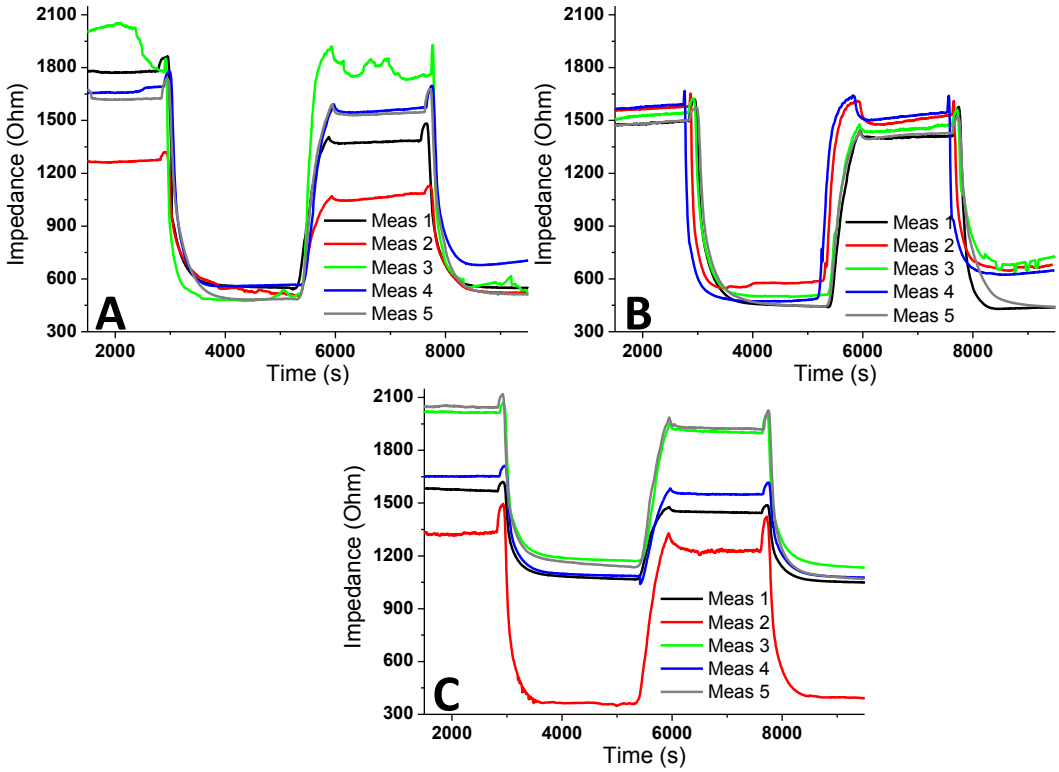

Figure 23: Impedance measurements for three different Si-samples at 2511 Hz, all 3 samples are made from solution 412.

The before mentioned factors do not explain the measured difference in impedance between the samples and within the measurements on one sample. To get a deeper understanding of the sample and its influence on EIS measurements, Nyquist plots were made. As the home-built flow cell setup only measured 3 decades of frequencies, measurements with the Iviumstat and HP 4194A impedance/gain-phase analyzer were performed after each EIS measurement. Figure 24 shows the Nyquist plots for the different elements of the biosensor

setup. Big differences are seen for the Nyquist plots for each step, which means that the surface of the Si-samples changes between and maybe even during measurements.

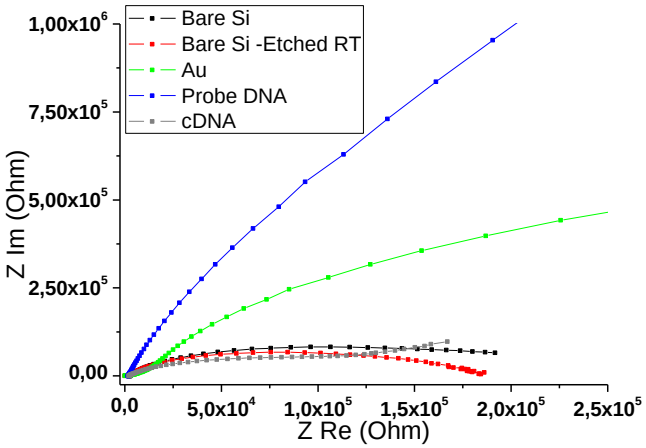

Figure 24: Nyquist plots for different elements of the setup, made out of data from Iviumstat and HP 4194A impedance/gain-phase analyzer measurements.

Therefore the chemical state of the sample assembly was thoroughly studied with XPS. Figure 25 shows a surface scan of a Si-sample (made from solution 473) right after etching and after 48h of storage in PBS. A magnification of figure 25 can be viewed at supplemental part 6 and 7. The survey scan after etching shows the presence of molybdenum, therefore it was not used for EIS measurements. The Au 4d-peaks are well defined, meaning that there are gold nanoparticles present on the substrate. When the sample resided 48h in 1x PBS the molybdenum and gold peaks are disappearing. Several other peaks became more evident, such as carbon and sodium. The presence of sodium and calcium is related to the storage in PBS and handling.

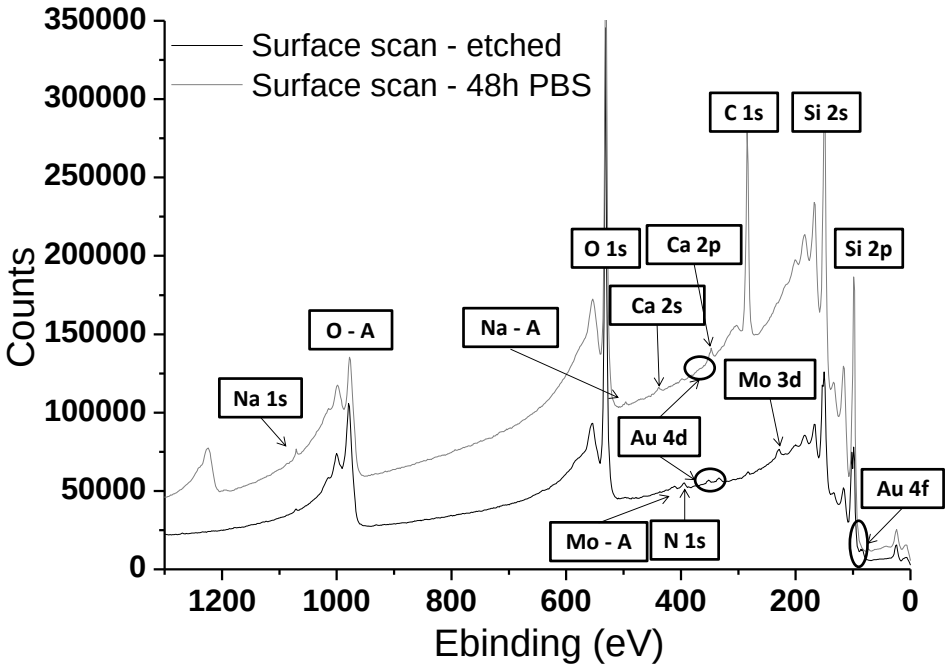

Figure 25: The surface scan was made with a pass energy of 187.85 eV. O - A and Mo - A are the auger peaks for oxygen and molybdenum, respectively.

The loss of the gold and silicon peaks after 48h of storage in PBS was studied more closely by looking at the Au 4f- (80 - 94 eV) and the Si 2p-peaks (98 - 108 eV) respectively. Figure 26 shows the Au 4f-peaks after etching and after 48h of storage in PBS. In this figure it can be seen that the amount of Au-nanoparticles is significantly decreased after storage in PBS. The peaks are also shifted to a higher binding energy; an indication that the present gold is in an higher positive oxidation state. This is a very important finding as it can influence the EIS measurements; less functionalized gold nanoparticles means that there is less dsDNA for denaturation.

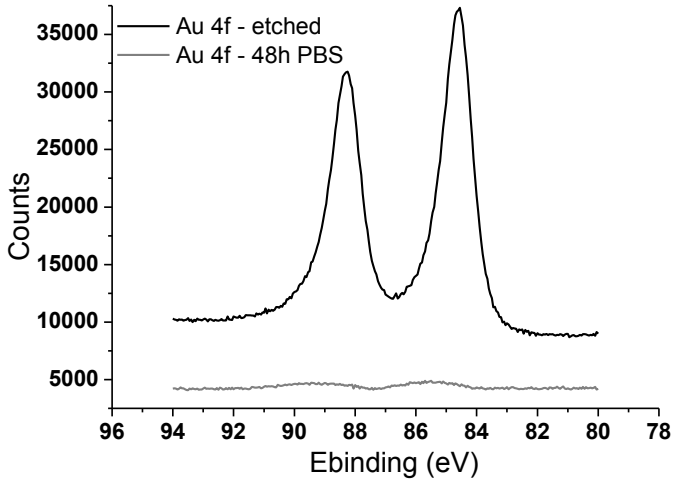

Figure 26: Measurement with XPS of Au 4f-peaks with a pass energy 23.5 eV right after etching and after 48h storage in PBS.

The question which arises now is why the gold gets removed from the substrate? After etching the gold is partially embedded in a SiO-layer. Figure 27 shows XPS measurements of Si 2p-peaks after etching and after residing 48h in 1x PBS. The figure shows that the oxide layer decreases after storage in PBS and a clear chemical shift is apparent. As the SiO-layer is decreased, the gold nanoparticles will not be embedded anymore.

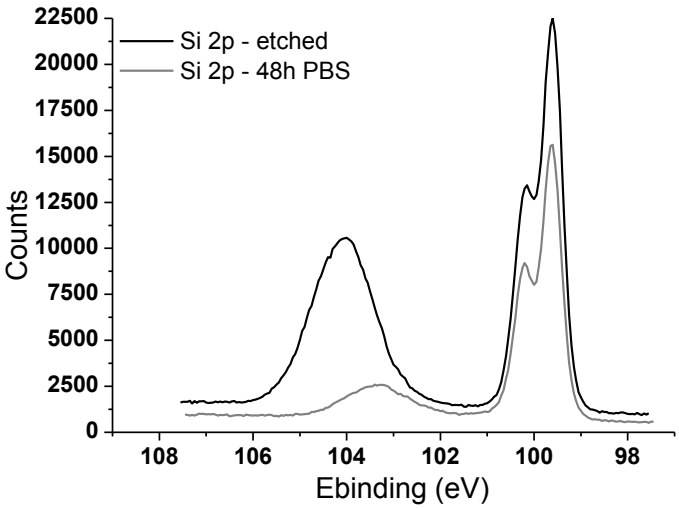

Figure 27: XPS measurement of Si 2p-peaks with a pass energy 5.85 eV right after etching and after 48h storage in PBS.

The repeatability of the measurements was not as expected (5.6% ± 1.25%). The deviation of 1.25% is a proof of this. The poor repeatability is due to the loss of gold nanoparticles and oxide layer. A possible reason for losing the oxide layer is the use of NaOH. Even at low temperature and low concentration of NaOH, it can have an etching effect on SiO_2[42]. The XPS results also show that the oxide layer gets smaller when the sample did not undergo an EIS cycle. Even storing in 1x PBS has already an effect on the oxide layer and therefore also on the amount of gold particles embedded in the oxide layer.

3.8) Tantalum pentoxide and diamond

Since Ta_2O_5 is known to be more electrochemically stable[43] than SiO_2, Ta_2O_5 was tried out as substrate. Measuring Ta_2O_5-substrates with the home-built flow-cell setup gave some issues which could not be resolved during this work. Figure 28A and B shows EIS measurement following a complete EIS cycle on a bare Ta_2O_5-substrate and on a Ta_2O_5-substrate with dsDNA, respectively. Both graphs are showing the impedance at 19952 Hz. The denaturation solvent used was 0.01 M NaOH. Because the ionic strength of 0.01 M NaOH is lower than that of 0.1 M NaOH, the temperature effect becomes more obvious (higher and broader overshoots).

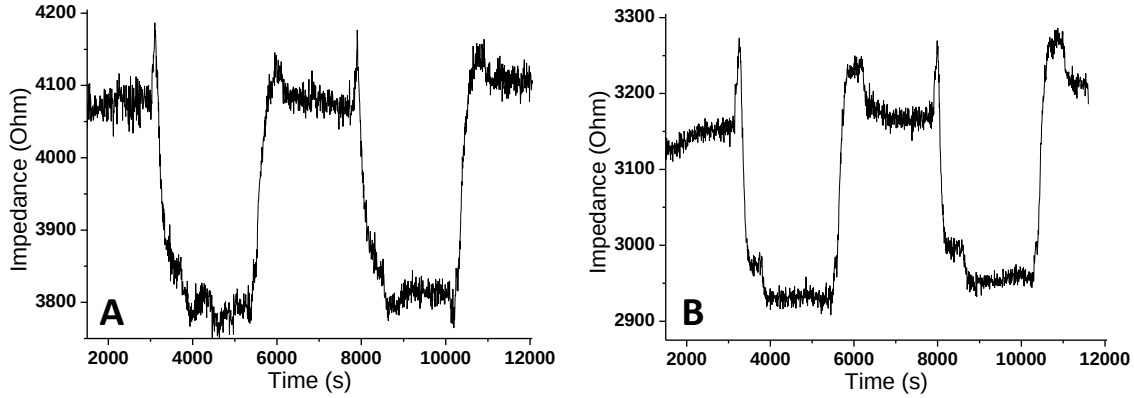

Figure 28: Impedance measurements following the denaturation cycle protocol of a Ta_2O_5-sample, shown frequency is 19952 Hz. A) bare sample. B) Ta_2O_5-substrate with dsDNA.

Unlike measurements with Si-substrates, with the Ta_2O_5-substrate there were problems measuring in the low frequency range, due to the low amplitude of the AC voltage (10 mV). At low frequencies the measurement is unreliable and shows a huge noise band. This problem might be avoided when using an impedance device with a higher AC voltage-amplitude, such as the HP 4194A analyzer. As the time was limited, only one measurement was performed to test this statement. However air in the measuring cell made this measurement unusable.

Normally the frequency chosen for the graphs is the frequency where the phase difference is the biggest. Also for the graphs of figure 28 this frequency was chosen, but because the lower frequencies are clouded by the noise band they cannot be taken into account. Therefore it is possible that the selected frequency is not the frequency that corresponds with the DNA-layer.

For the Ta_2O_5-substrate also measurements with the Iviumstat and HP 4194A impedance/gain-phase analyzer were performed for a bare substrate before and after a typical EIS cycle, for a sample with probe DNA and for a sample after denaturation inside the home-built flow cell setup. These Nyquist plots (figure 29) also show that the surface of the Ta_2O_5-substrate was changing during preparation or measurements. The surface of the Ta_2O_5-substrates was also studied with XPS. The preliminary XPS results show contamination with aluminum, which is from the substrate (aluminum was used as used as a buffer layer during the preparation of Ta_2O_5-substrate) itself. It is not clear how the aluminum came on to the surface; it could come from the sides of the substrate during washing or due to the cracks in the substrate itself. The effect of the aluminum is unclear on the EIS measurements.

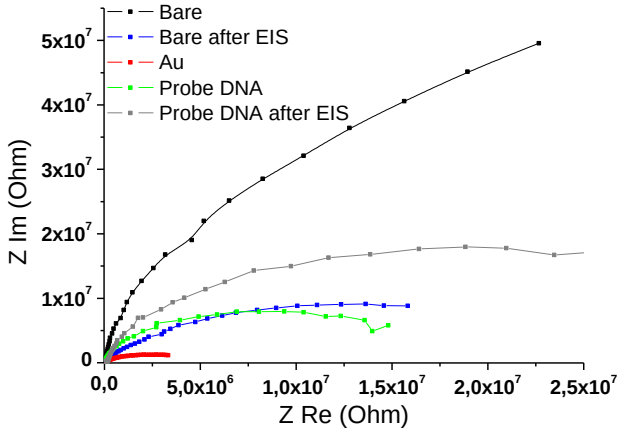

Figure 29: Nyquist plots for different elements of the setup on a Ta_2O_5-substrate.

Due to time limitations it was decided to continue with diamond substrates, which are known to be electrochemically stable. Only preliminary experiments will be presented in this work. Figure 30 shows the Nyquist plots for the different elements of the setup on a diamond substrate. While for both Si- and Ta_2O_5-substrates the Nyquist plots differ before and after EIS measurement (following a complete denaturation cycle protocol) significantly, it does not for the diamond substrate as can be seen from the Nyquist plots of probe DNA before and after EIS measurement. This is a first indication that the diamond substrate is stable throughout the process.

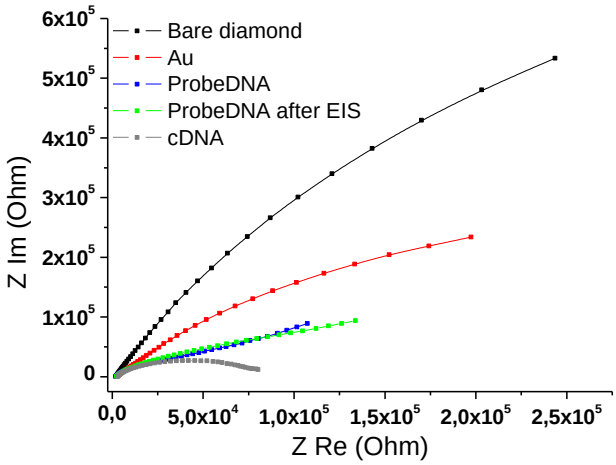

Figure 30: Nyquist plots for different elements of the setup on a diamond substrate.

Simultaneously with the Iviumstat and HP 4194A impedance/gain-phase analyzer-measurements, also measurements with the home-built flow cell setup were performed for the diamond-substrates. Figure 31 shows a typical denaturation cycle for each element of the setup. The effect size for bare diamond, gold nanoparticles on diamond and gold nanoparticles functionalized with probe DNA is 3.6%, 3.0% and 2.6%, respectively. This is significantly lower than the effect size of denaturation, which is 12.6%. As a general trend, the impedance at PBS stabilization step 5 is at a lower impedance value for all the elements than at stabilization step 1. A possible reason for the lower impedance level of stabilization time 5 compared to the impedance at stabilization time 1, for all the different individual components of the setup, is that the hydrogen termination on the diamond might be exchanged by the OH-groups of the NaOH. However, this needs further investigation.

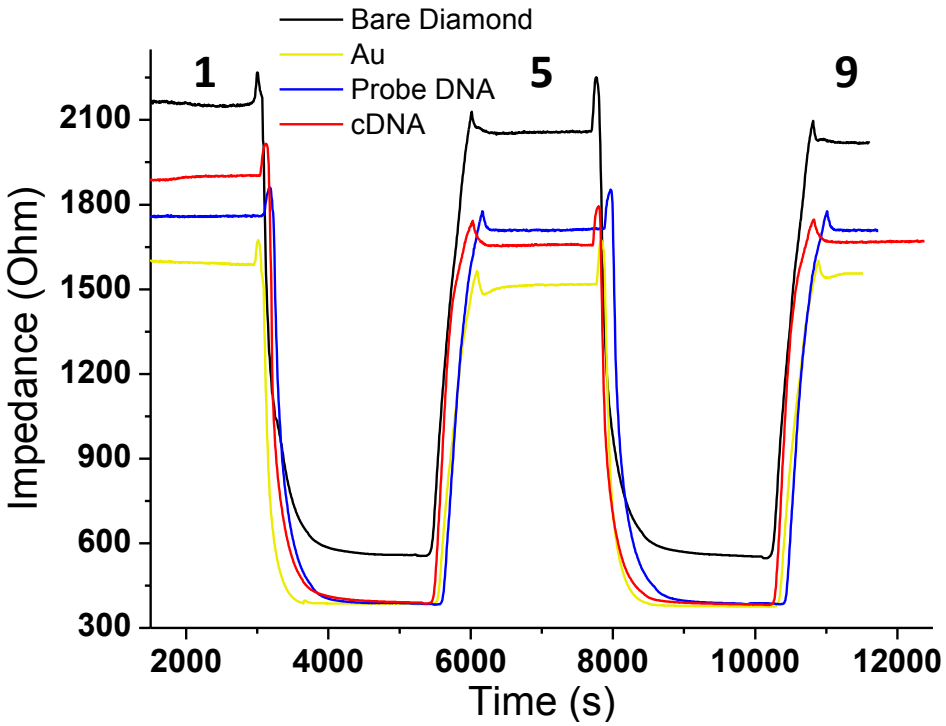

Figure 31: EIS measurement of different components in a typical denaturation experiment. Diamond sample made with micellar approach from solution 518.

4) Conclusion

For the first time, nanostructures produced using the micellar approach were used to immobilize DNA by physical absorption for further use in biosensing employing EIS. An highly ordered array of gold nanoparticles were used as immobilization platform for attaching probe DNA, to further use it for studying the denaturation of hybridized DNA, as a first step towards the detection of SNP's. As the use of linker molecules, long preparation times and the need for complex chemistry are avoided, this biosensor will be more easy and faster to use and can be used as an alternative to the currently used biosensor platform based on fatty acid coupling. The attachment of fatty acid to diamond is a lengthy procedure requiring a minimum of 20 hours of photochemical treatment, followed by attachment of probe DNA by EDC-coupling. Additionally, several cleaning steps with different protocols are required.

This thesis proves that it is possible to create a nanoparticle based biosensor without the need for a linker molecule when attaching DNA, nor the need for long preparation procedures. Using the micellar approach, gold salt loaded micellar solution was prepared. The first problem encountered during this thesis was when micelles needed to be dip-coated on the bigger substrates. The previously optimized setup for dip-coating had to be redesigned for substrates that fits the home-built fluid cell setup for the EIS measurements as well as the sample holder in the plasma etcher. After optimizing the dip-coating procedure high hexagonal order was also obtained for the bigger substrates. The dip-coated samples were etched with O- and H-plasma and characterized with AFM and XPS before measuring with EIS. During a typical denaturation cycle PBS and NaOH are interchanged in the flow cell setup. After stabilization in PBS, NaOH is pumped into the flow cell to denature the dsDNA. The NaOH and denatured DNA is washed out of the cell with PBS. After a stabilization period, NaOH is pumped into the flow cell again, to see the effect of the solvent alone on the impedance measurement. Finally the cell is again rinsed with PBS, when doing this it can be seen if the denaturation due to NaOH was completed during the first NaOH-pumping.

The measurements on the Si-samples clearly showed comparable results with research performed by Van Grinsven et al.[5]. The effect size of denaturation was 5.6% ± 1.25 for the Si-samples, but the repeatability of the measurements was not as expected. The deviation of 1.25% is a proof of this. The poor repeatability is due to the loss of gold nanoparticles and oxide layer. A possible reason for losing the oxide layer is the use of NaOH, as even at low temperature and low concentration of NaOH, it can have an etching effect on SiO_2[42]. The XPS results show that the oxide layer gets smaller even when the sample did not undergo a typical EIS denaturation cycle. It was found that even storing in 1x PBS has an adverse effect on the oxide layer and therefore also on the gold particles embedded in the oxide layer.

During the EIS measurements on the Ta_2O_5 based samples, a fundamental problem was seen due to the low amplitude of the measuring voltage. Also the XPS results show an unexpected contamination with aluminum and the effect of contaminants on EIS is unclear. These factors made the analyzing of the EIS measurements on the Ta_2O_5 based samples difficult.

Measuring the EIS cycle for the diamond samples showed promising results. Analyzing the Nyquist plots showed that diamond is electrochemically stable during the process. Further study on the diamond based samples are required to show if the repeatability of the measurements can be guaranteed.

Although repeatability was a problem, the measurements show a proof of principle of the nanoparticle-based biosensor setup. In this work it was shown that DNA is attached to the gold nanoparticles and that NaOH denatures the dsDNA during an typical EIS cycle. Figure 21 and 32 (in Results and Discussion) show that during the denaturation cycle, the impedance value at the last stabilizing step in PBS (figure 21, step 9) is at the same value as in the second stabilizing step in PBS (figure 21, step 5), Nevertheless, both figures show a higher impedance value in the first stabilization period in PBS (figure 21, step 1). This means that the NaOH indeed denatures all the dsDNA, but within the short measuring time it does not affect the substrate; otherwise the last PBS stabilization step would differ from the second stabilization step.

To improve the consistency of the sensor surface during the measurement as well to reuse the sensor, it is important to study which part of the process right from the functionalization until the completion of EIS measurement affects the oxide layer and to what extent. One possibility to improve reusability is storing the samples in a different solvent (0.9% NaCl-solution) or in the dried state. Also, the removal of excess DNA could be performed by washing with purified water instead of using other solvents. It could also be considered to denature the samples by increasing temperature (Van Grinsven et al.) or use a pure EIS read-out of hybridization experiments without changing solvents[18]. Another possibility is using a substrate that is not affected by the used solvents; preliminary measurements in this work show that diamond is a valid option. For future studies, the analysis of EIS and XPS results after each step will help to deduce the influence of different factors and understand the experiments better.

If the before mentioned issues with consistency and reusability is resolved, then particle size and interparticle distance can be optimized. The optimization of nanoparticle size will provide a genetic test with outstanding sensitivity. It would also be important to measure the amount of DNA bound to the gold nanoparticles, so that the difference in measurements for different sizes of nanoparticles can be well understood. Because of the possible miniaturization of such biosensors, massive parallel screening at point-of-care becomes possible with small sample volumes. This will greatly improve the speed and the efficiency of health care.

Reference

1. Fischer, S.G. and L.S. Lerman, *Separation of random fragments of DNA according to properties of their sequences.* Proceedings of the National Academy of Sciences, 1980. **77**(8): p. 4420-4424.
2. Southern, E.M., *Detection of specific sequences among DNA fragments separated by gel electrophoresis.* Journal of Molecular Biology, 1975. **98**(3): p. 503-517.
3. Schena, M., et al., *Quantitative Monitoring of Gene Expression Patterns with a Complementary DNA Microarray.* Science, 1995. **270**(5235): p. 467-470.
4. Jonsson, U., et al., *Real-time biospecific interaction analysis using surface plasmon resonance and a sensor chip technology.* BioTechniques, 1991. **11**(5): p. 620-7.
5. Van Grinsven, B., et al., *Rapid assessment of the stability of DNA duplexes by impedimetric real-time monitoring of chemically induced denaturation.* Lab on a Chip, 2011. **11**(9): p. 1656-1663.
6. Xia, Y., et al., *One-Dimensional Nanostructures: Synthesis, Characterization, and Applications.* Advanced Materials, 2003. **15**(5): p. 353-389.
7. Whyman, R., *Gold nanoparticles: a renaissance in gold chemistry* Gold Bulletin, 1996. **29**(1): p. 11-15.
8. Xu, K., et al., *Recent Development of Nano-Materials Used in DNA Biosensors.* Sensors, 2009. **9**(7): p. 5534-5557.
9. Paciotti, G.F., D.G.I. Kingston, and L. Tamarkin, *Colloidal gold nanoparticles: a novel nanoparticle platform for developing multifunctional tumor-targeted drug delivery vectors.* Drug Development Research, 2006. **67**(1): p. 47-54.
10. Michalet, X., et al., *Quantum Dots for Live Cells, in Vivo Imaging, and Diagnostics.* Science, 2005. **307**(5709): p. 538-544.
11. Drake, C., et al., *Metallic nanostructured materials based sensors.* International Materials Reviews, 2007. **52**(5): p. 289-317.
12. Wilson, R., *The use of gold nanoparticles in diagnostics and detection.* Chemical Society Reviews, 2008. **37**(9): p. 2028-2045.
13. El-Sayed, I.H., X. Huang, and M.A. El-Sayed, *Surface Plasmon Resonance Scattering and Absorption of anti-EGFR Antibody Conjugated Gold Nanoparticles in Cancer Diagnostics: Applications in Oral Cancer.* Nano Letters, 2005. **5**(5): p. 829-834.
14. Eustis, S. and M.A. El-Sayed, *Why gold nanoparticles are more precious than pretty gold: Noble metal surface plasmon resonance and its enhancement of the radiative and nonradiative properties of nanocrystals of different shapes.* Chemical Society Reviews, 2006. **35**(3): p. 209-217.
15. Hutter, E. and M.-P. Pileni, *Detection of DNA Hybridization by Gold Nanoparticle Enhanced Transmission Surface Plasmon Resonance Spectroscopy.* The Journal of Physical Chemistry B, 2003. **107**(27): p. 6497-6499.
16. Macdonald, J.R., *Impedance Spectroscopy.* Annals of Biomedical Engineering, 1992. **20**: p. 289-305.
17. Kafka, J., et al., *A label-free DNA sensor based on impedance spectroscopy.* Electrochimica Acta, 2008. **53**(25): p. 7467-7474.

18. Cai, W., et al., *Direct electrical detection of hybridization at DNA-modified silicon surfaces.* Biosensors and Bioelectronics, 2004. **19**(9): p. 1013-1019.
19. Ozin, G., A. Arsenault, and L. Cademartiri, *Nanochemistry: A chemical approach to nanomaterials*. 2 ed. 2008: The Royal Society of Chemistry.
20. Wegner, K. and et al., *Cluster beam deposition: a tool for nanoscale science and technology.* Journal of Physics D: Applied Physics, 2006. **39**(22): p. R439.
21. Ethirajan, A., et al., *A Micellar Approach to Magnetic Ultrahigh-Density Data-Storage Media: Extending the Limits of Current Colloidal Methods.* Advanced Materials, 2007. **19**(3): p. 406-410.
22. Kästle, G., et al., *Micellar Nanoreactors—Preparation and Characterization of Hexagonally Ordered Arrays of Metallic Nanodots.* Advanced Functional Materials, 2003. **13**(11): p. 853-861.
23. Attension. *Critical Micelle Concentration*. 2009; Available from: http://www.attension.com/critical-micelle-concentration.aspx.
24. Tieleman, D.P., D. van der Spoel, and H.J.C. Berendsen, *Molecular Dynamics Simulations of Dodecylphosphocholine Micelles at Three Different Aggregate Sizes: Micellar Structure and Chain Relaxation.* The Journal of Physical Chemistry B, 2000. **104**(27): p. 6380-6388.
25. Bansmann, J., et al., *Controlling the Interparticle Spacing of Au−Salt Loaded Micelles and Au Nanoparticles on Flat Surfaces.* Langmuir, 2007. **23**(20): p. 10150-10155.
26. Gilb, S., et al., *Cavity ring-down spectroscopy of metallic gold nanoparticles.* The European Physical Journal D, 2007. **45**(3): p. 501-506.
27. Weigl, F., et al., *From self-organized masks to nanotips: A new concept for the preparation of densely packed arrays of diamond field emitters.* Diamond and Related Materials, 2006. **15**(10): p. 1689-1694.
28. NT-MDT. *The Hooke's Law*. 1998; Available from: http://www.ntmdt.com/spm-basics/view/hooke-law.
29. Rugar, D. and P. Hansma, *Atomic Force Microscopy.* Physics Today, 1990: p. 23-30.
30. Meyer, E., *Atomic Force Microscopy.* Progress in Surface Science, 1992. **41**: p. 3-49.
31. Li, H.-Q. *Atomic Force Microscopy*. 1998; Available from: http://www.chembio.uoguelph.ca/educmat/chm729/afm/firstpag.htm.
32. Wu, W. *X-ray Photoemission Spectrometry (XPS)*. 2010; Available from: http://www.hkbu.edu.hk/~csar/xps.html.
33. Winograd, N. and S.W. Gaarenstroom, *X-Ray Photoelectron Spectroscopy*. Physical Methods in Modern Chemical Analysis, 1980. **2**: p. 115-169.
34. Kuphaldt, T.R., *Lessons In Electric Circuits*. 2006.
35. Katz, E. and I. Willner, *Probing Biomolecular Interactions at Conductive and Semiconductive Surfaces by Impedance Spectroscopy: Routes to Impedimetric Immunosensors, DNA-Sensors, and Enzyme Biosensors.* Electroanalysis, 2003. **15**(11): p. 913-947.
36. Scott, C. *The RCA Cleaning Process*. 1998; Available from: http://www.bold-tech.com/technical/rca_cleaning.html.
37. Bachman, M. *RCA-1 Silicon Wafer Cleaning*. INRF application note 1999; Available from: http://www.physics.ubc.ca/~ampel/nanofab/sop/rca-clean-1.pdf.

38. Bachman, M. *RCA-2 Silicon Wafer Cleaning*. INRF application note 2002; Available from: http://www.physics.ubc.ca/~ampel/nanofab/sop/rca-clean-2.pdf.
39. Van Grinsven, B., et al., *Customized impedance spectroscopy device as possible sensor platform for biosensor applications.* Physica Status Solidi (a), 2010. **207**(4): p. 919-923.
40. Nečas, D. and P. Klapetek. *Gwyddion*. 2010; Available from: http://gwyddion.net/.
41. Wenmackers, S., et al., *Diamond-based DNA sensors: surface functionalization and read-out strategies.* physica status solidi (a), 2009. **206**(3): p. 391-408.
42. Seidel, H., et al., *Anisotropic Etching of Crystalline Silicon in Alkaline Solutions.* Journal of The Electrochemical Society, 1990. **137**(11): p. 3612-3626.
43. Platen, J., A. Poghossian, and M. Schöning, *"Microstructured Nanostructures" – Nanostructuring by Means of Conventional Photolithography and Layer-expansion Technique.* Sensors, 2006. **6**(4): p. 361-369.

Supplemental part

Part 1: RCA-1 Silicon Wafer Cleaning

RCA-1 Silicon Wafer Cleaning

INRF application note
Process name: RCA01

Mark Bachman
Fall 1999

Overview

The famous RCA-1 clean (sometimes called "standard clean-1", SC-1), developed by Werner Kern at RCA laboratories in the late 1960's, is a procedure for removing organic residue and films from silicon wafers. The decontamination works based on sequential oxidative desorption and complexing with H_2O_2-NH_4OH-H_2O (RCA1). A second RCA-2 clean (SC-2) is often used H_2O_2-HCl-H_2O to further clean the surface. RCA-1 clean is used to remove organic residues from silicon wafers. In the process, it oxidizes the silicon and leaves a thin oxide on the surface of the wafer which should be removed is a pure silicon surface is desired.

This is a level-1 process and requires basic INRF safety certification. The use of dangerous chemicals requires that the user may not perform the process alone.

Time needed

This process takes 30 minutes to complete in total.

Materials needed

- ❑ Ammonium hydroxide
- ❑ Hydrogen peroxide
- ❑ Pyrex bath containers
- ❑ Hot plate

Preparation

Setup time for this process is about 5 minutes. This process takes about 20 minutes to complete. The general recipe is for RCA-1 cleanser is: 5 parts water (H_2O), 1 part 27% ammonium hydroxide (NH_4OH), 1 part 30% hydrogen peroxide (H_2O_2).

325 ml DI water
65 ml NH_4OH (27%)
65 ml H_2O_2 (30%)

Procedure [RCA-1]

Put 325 ml DI water in a Pyrex beaker, add 65 ml NH_4OH (27%) and then heat to 70±5° C on hot plate. Remove from hot plate and add 65 ml H_2O_2 (30%). Solution will bubble vigorously after 1–2 minutes, indicating that it is ready for use. Soak the silicon wafer in the solution for 15 minutes. When finished, transfer the wafer to a container with overflowing DI water from a tap to rinse and remove the solution. After several water changes, remove the wafer under flowing water. (Still water surface can contain organic residue that will redeposit on the wafer surface when removing wafer.)

Clean up

To dispose of the RCA-1 solution, dilute with cold water, let cool and sit for 10 minutes, then pour down the drain with plenty of cold water to flush. Old RCA cleaning solution cannot be used since it loses its effectiveness in 24 hours at room temperature (30 minutes at 70°C). Rinse all labware three times in clean water.

Safety and emergency

All INRF safety and procedural regulations must be followed. Review the INRF standard operating procedures for fire, chemical spill, and chemical exposure. Use of RCA requires at least one other person in the clean room (buddy system). RCA clean should be performed in a laminar flow bench, using nitrile gloves and eye protection.

Hydrogen peroxide is an explosive chemical. Never leave the RCA process unattended. Do not store the hydrogen peroxide near the hotplate or any other source of heat. Any small spills should be wiped up immediately with wipes. Dispose the wipes in the corrosive waste container.

In case of exposure to skin or eyes, flush immediately with water for 15 minutes. Remove all clothing that are exposed and flush with water. Report to INRF staff or report to EH&S. Seek medical attention to ensure that the burns are minimal.

In case of large spill, follow the INRF Standard Operating Procedure for chemical spills.

References

Kevin M. Walsh, *University of Louisville Standard Operating Procedures*, http://mitghmr.spd.louisville.edu/lutz/resources/sops/

Prudent Practices in the Laboratory, National Research Council, 1995.

W. Kern and J. Vossen, Eds., *Thin Film Processes*, Academic Press: New York, 1978, Ch V-1.

W. Kern, Ed., *Handbook of Semiconductor Cleaning Technology*, Noyes Publishing: Park Ridge, NJ, 1993, Ch 1.

Part 2: RCA-2 Silicon Wafer Cleaning

RCA-2 Silicon Wafer Cleaning

INRF application note
Process name: RCA02

Mark Bachman
Spring 2002

Overview

The famous RCA-2 clean (sometimes called "standard clean-2", SC-2), developed by Werner Kern at RCA laboratories in the late 1960's, is a procedure for removing metal ions from silicon wafers. The decontamination works based on sequential oxidative desorption and complexing with H_2O_2-NCl-H_2O (RCA-2). Typically this is preceded by an RCA-1 clean (SC-1, H_2O_2-NH_4OH-H_2O) to remove organic residues. In the process, it oxidizes the silicon and leaves a thin oxide on the surface of the wafer.

This is a level-1 process and requires basic INRF safety certification. The use of dangerous chemicals requires that the user may not perform the process alone.

Time needed

This process takes 30 minutes to complete in total.

Materials needed

- ❑ Hydrogen chloride
- ❑ Hydrogen peroxide
- ❑ Pyrex bath containers
- ❑ Hot plate

Preparation

Setup time for this process is about 5 minutes. This process takes about 20 minutes to complete. The general recipe is for RCA-2 cleanser is: 6 parts water (H_2O), 1 part 27% hydrogen chloride (HCl). 1 part 30% hydrogen peroxide (H_2O_2).

300 ml DI water
50 ml HCl
50 ml H_2O_2 (30%)

Procedure [RCA-2]

Put 300 ml DI water in a Pyrex beaker, carefully add 50 ml HCl and then heat to 70±5° C on hot plate. Remove from hot plate and add 50 ml H_2O_2 (30%). Solution will bubble vigorously after 1–2 minutes, indicating that it is ready for use. Soak the silicon wafer in the solution for 10 minutes. When finished, remove the wafer and rinse with clean DI water.

Clean up

To dispose of the RCA-2 solution, let cool to room temperature. Then pour in INRF labeled waste container. Close, but do not tighten, waste lid to allow escape of any additional gases that might be generated.

Safety and emergency

All INRF safety and procedural regulations must be followed. Review the INRF standard operating procedures for fire, chemical spill, and chemical exposure. Use of RCA-2 requires at least one other person in the clean room (buddy system). RCA-2 clean should be performed in a laminar flow bench, using nitrile gloves and eye protection.

Hydrogen peroxide is an explosive chemical. Never leave the RCA process unattended. Do not store the hydrogen peroxide near the hotplate or any other source of heat. Any small spills should be wiped up immediately with wipes. Dispose the wipes in the corrosive waste container.

In case of exposure to skin or eyes, flush immediately with water for 15 minutes. Remove all clothing that are exposed and flush with water. Report to INRF staff or report to EH&S. Seek medical attention to ensure that the burns are minimal.

In case of large spill, follow the INRF Standard Operating Procedure for chemical spills.

References

Prudent Practices in the Laboratory, National Research Council, 1995.

W. Kern and J. Vossen, Eds., *Thin Film Processes*, Academic Press: New York, 1978, Ch V-1.

W. Kern, Ed., *Handbook of Semiconductor Cleaning Technology*, Noyes Publishing: Park Ridge, NJ, 1993, Ch 1.

Part 3: AFM images of samples dip-coating with non-optimized bottle

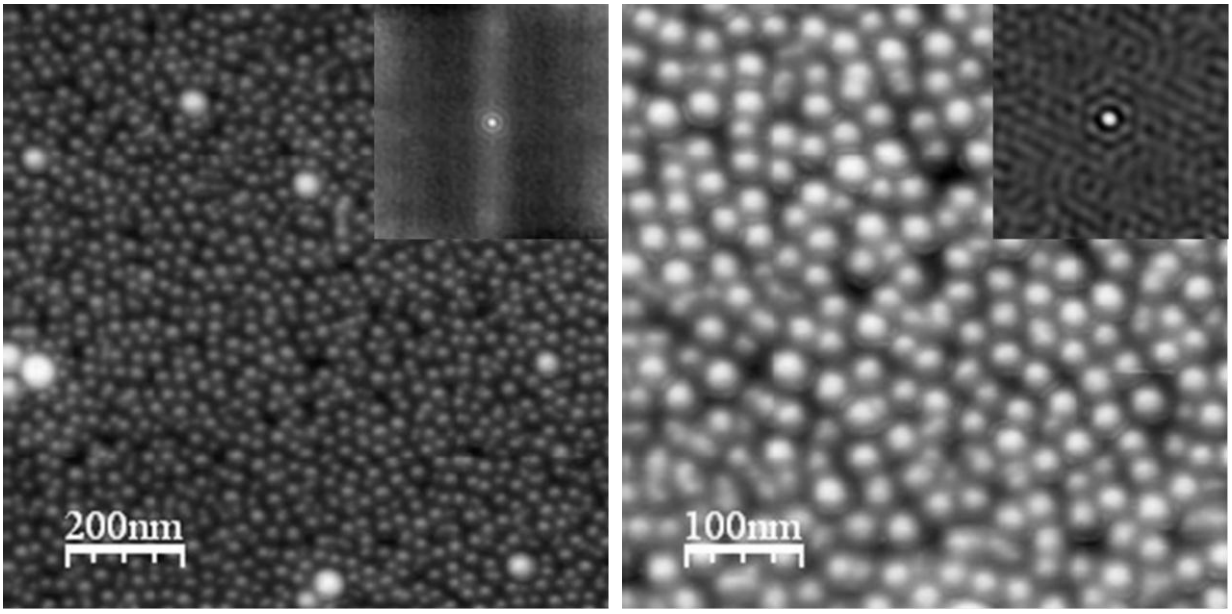

The morphology of micelles dip-coated on a Si-substrate from a non-optimized bottle. Solution 404 was used to dip-coat this sample, the solution was prepared with the micellar approach. The image shows two AFM measurements with a different magnification.

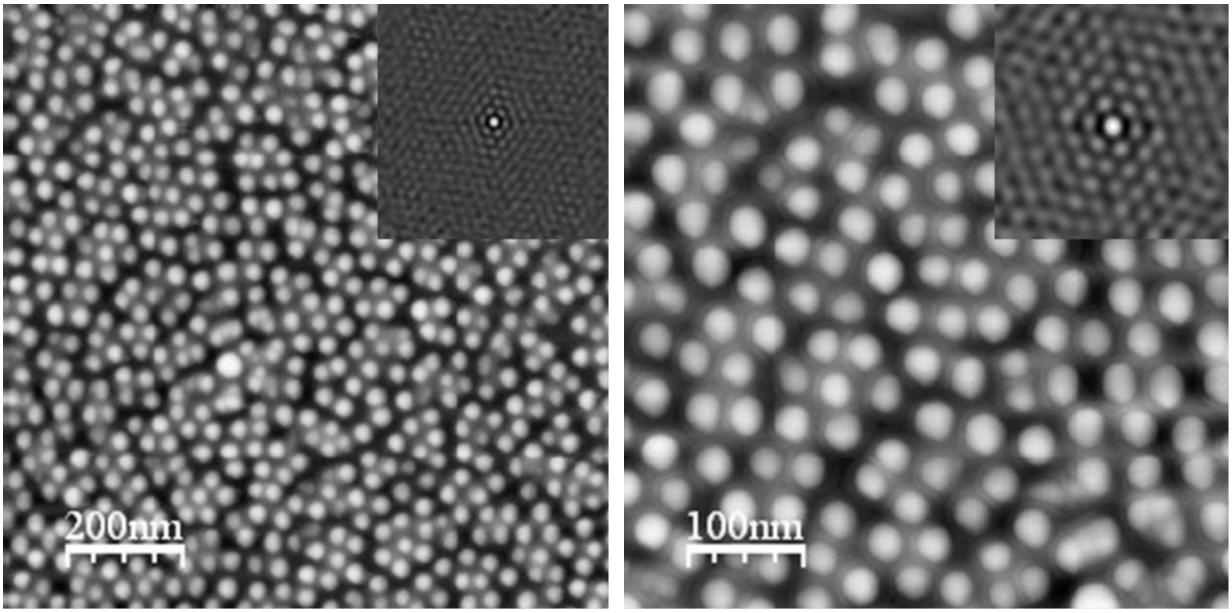

The morphology of micelles dip-coated on a Si-substrate from the optimized bottle but no cap. Solution 404 was used to dip-coat this sample, the solution was prepared with the micellar approach. The image shows two AFM measurements with a different magnification.

Part 4: AFM images of etched samples

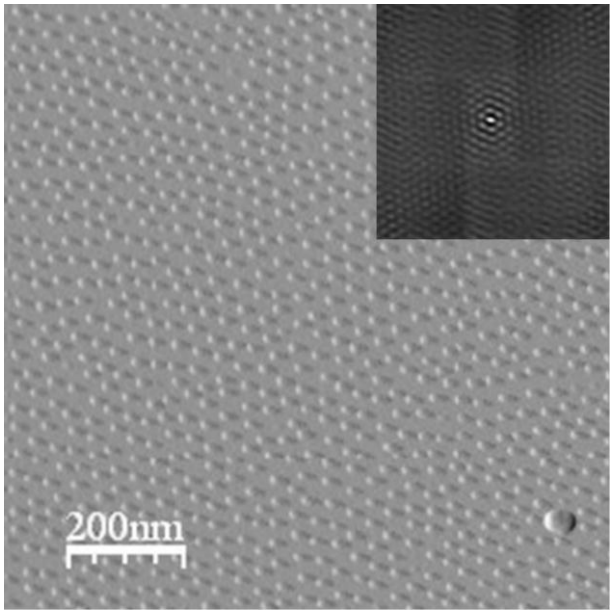

The morphology of gold nanoparticles on a Si-substrate after etching. The nanoparticles were prepared with the micellar approach, solution 412. The Gwyddion software counted 609 particles for 1 μm^2, with an interparticle distance of 42 nm and an average particle size of 2.7 nm.

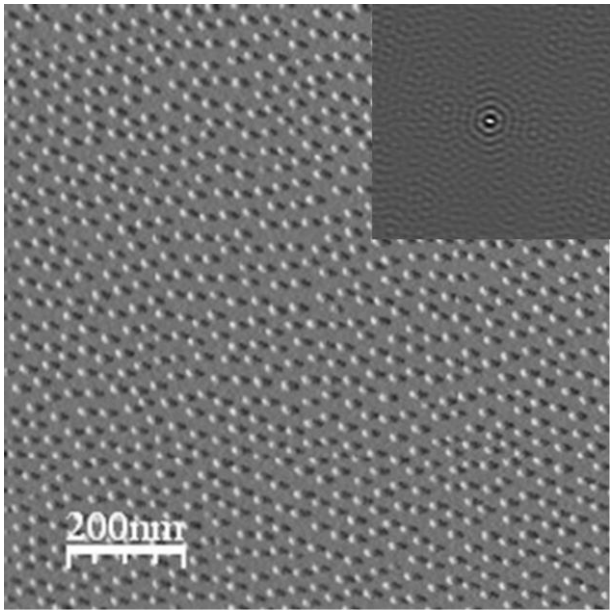

The morphology of gold nanoparticles on a Si-substrate after etching. The nanoparticles were prepared with the micellar approach, solution 418. The Gwyddion software counted 624 particles for 1 μm^2, with an interparticle distance of 37 nm and an average particle size of 2.6 nm.

Part 5: EIS measurements at a pumping speed of 0.25 ml/min

The effect size is dependent on the amount of nanoparticles present for functionalization and the amount of denatured DNA. The optimized pumping speed of 0.25 ml/min for the diamond-based setup was also used for the first impedance measurements for the nanoparticle based setup. As can be seen in the below figures the measurements had an unexpected result: the impedance kept on changing over-time which means that the surface of the sample was also altered at each step. Therefore the pumping speed was lowered to 0.125 ml/min (figure 23, in Results and Discussion).

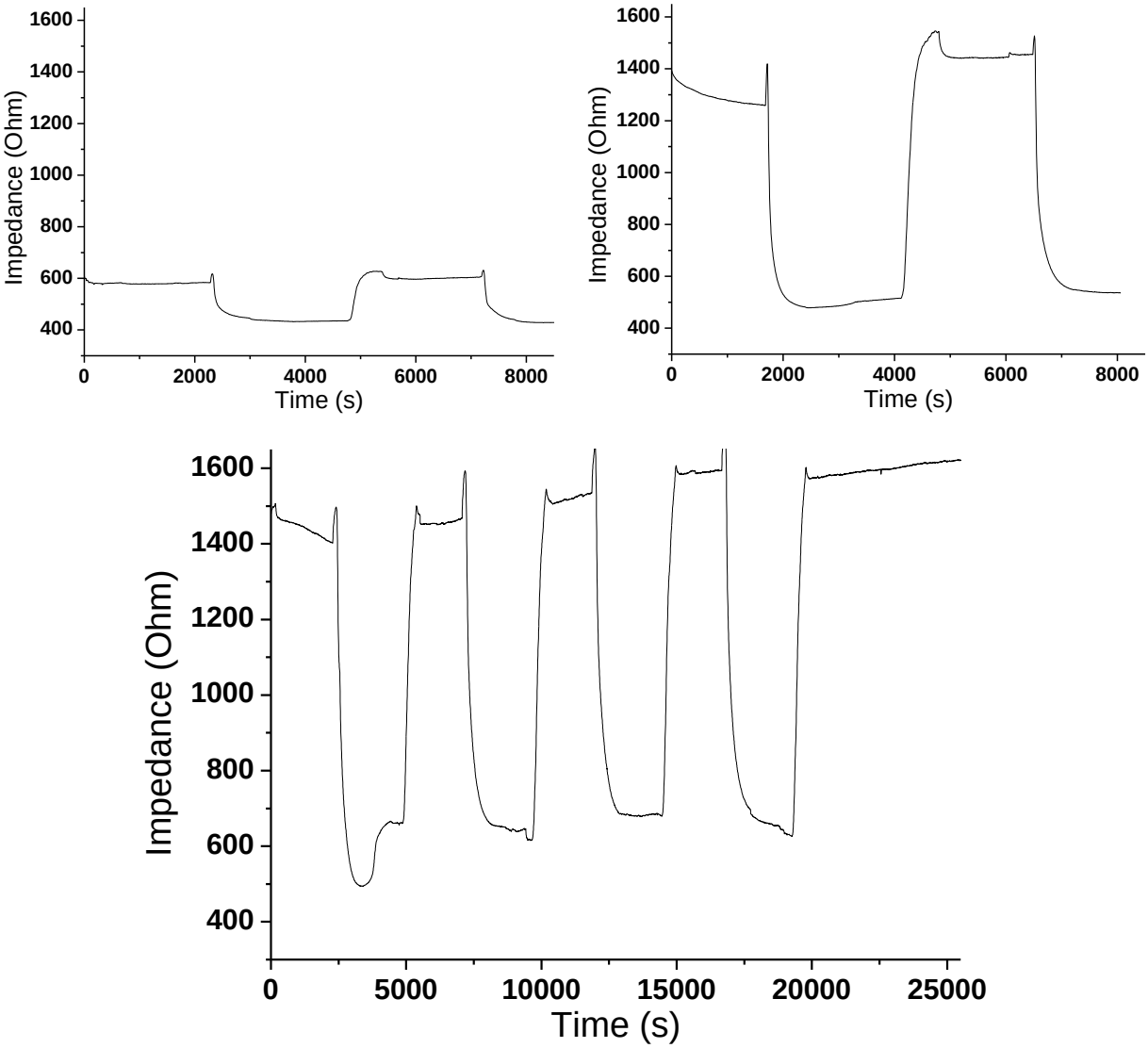

The figures shows impedance measurements for 3 different Si-samples at 2511 Hz and with a programmed pumping speed of 0.25 ml/min. All 3 samples were made from solution 404. The last sample was measured over a longer time to see the time-dependent effect. Overall it can be seen that the impedance rises over time.

Part 6: Surface scan with XPS of a Si-sample after etching

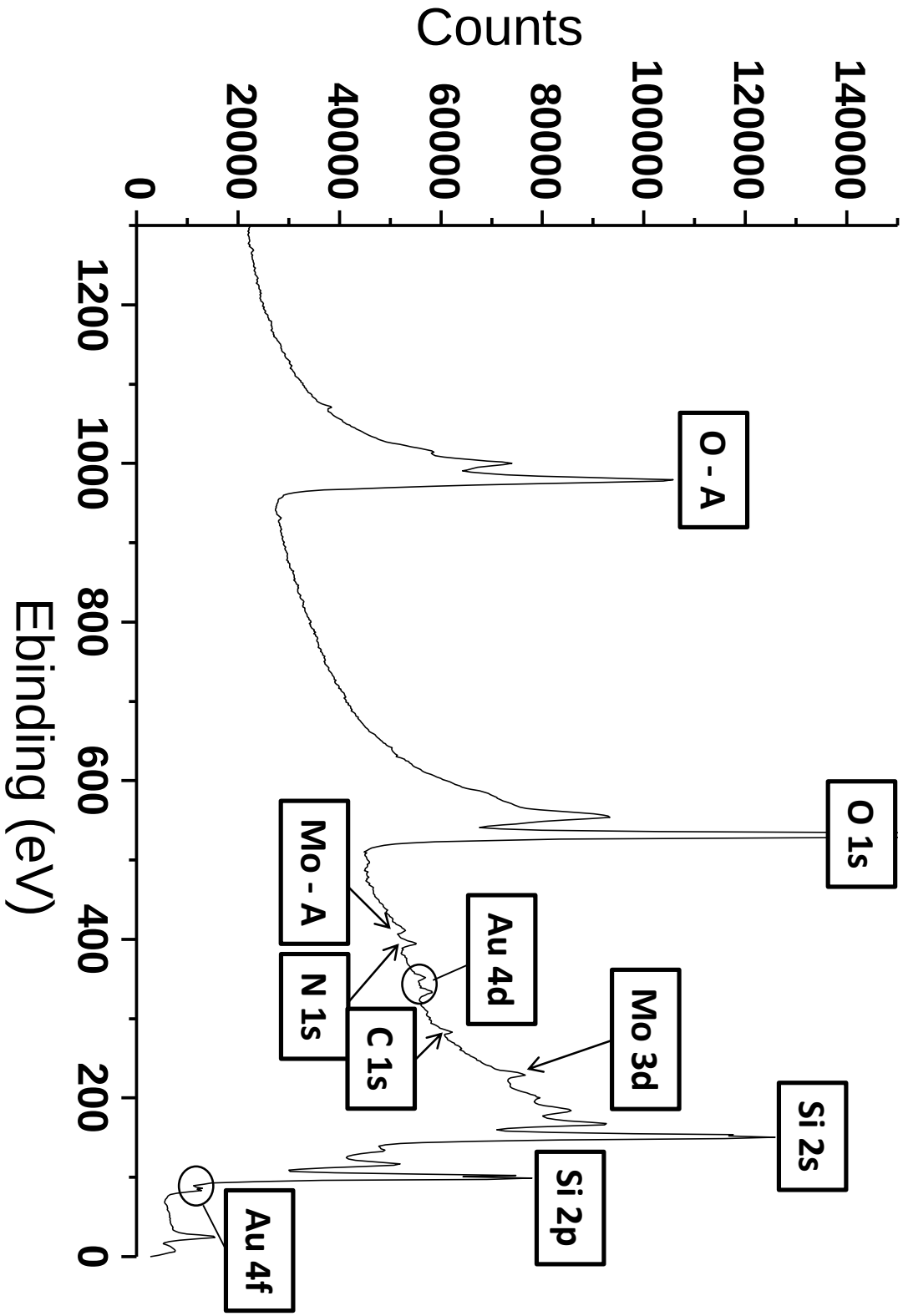

The surface scan was made with a pass energy of 187.85 eV. O - A and Mo - A are the auger peaks for oxygen and molybdenum, respectively. This survey scan shows the presence of some contaminants, like molybdenum. The Au 4d peaks are good to see, meaning that there are gold nanoparticles present on the substrate.

Part 7: Surface scan with XPS of a Si-sample after etching and storage in PBS

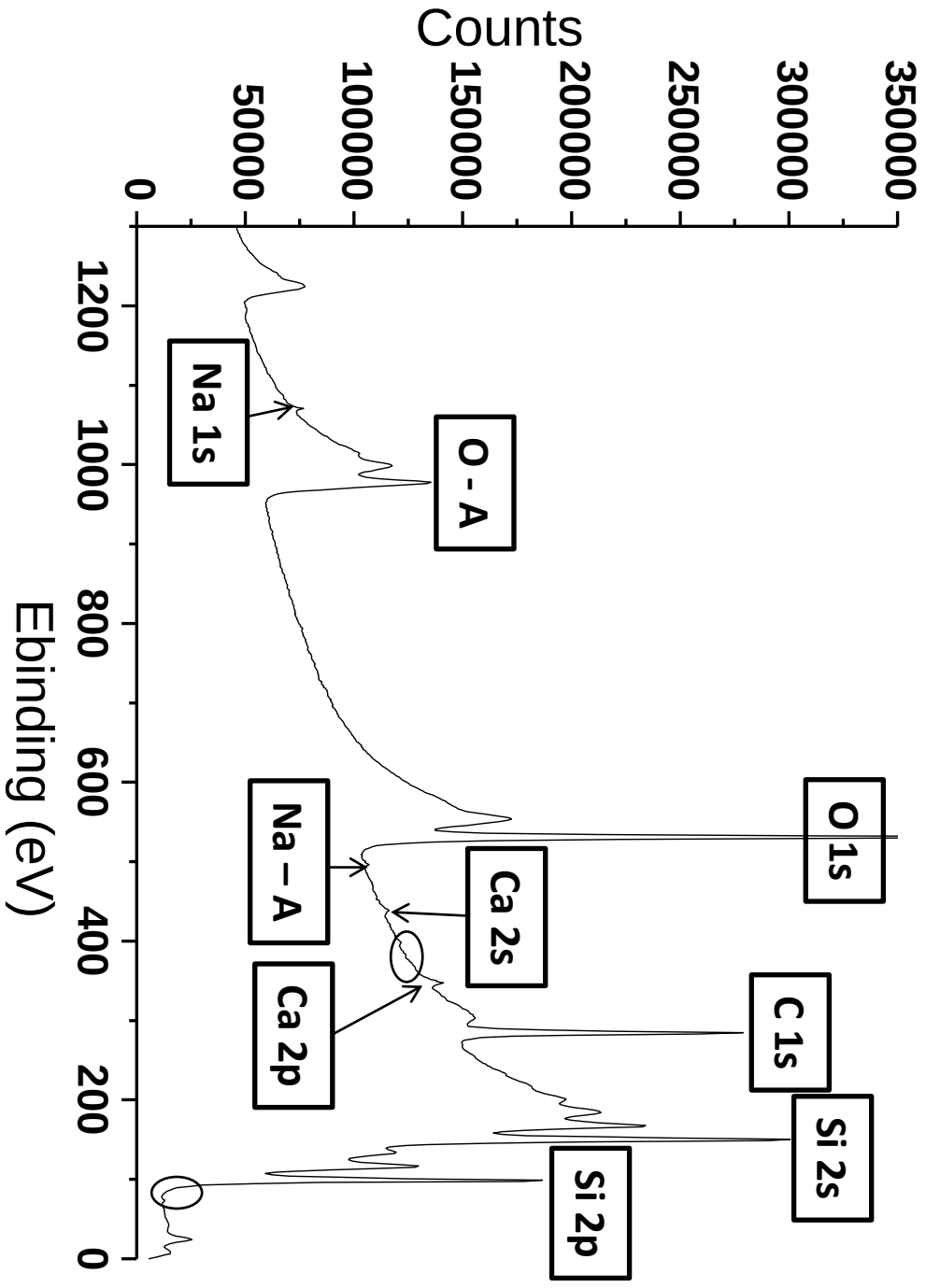

The surface scan was made with a pass energy of 187.85 eV. O - A and Na - A are the auger peaks for oxygen and sodium, respectively. This survey scan shows that the Au 4d- and Au 4f-peaks are not distinguishable anymore (circles). There is no more molybdenum present on the surface. Instead there are other chemicals present such as calcium and sodium.

Auteursrechtelijke overeenkomst

Ik/wij verlenen het wereldwijde auteursrecht voor de ingediende eindverhandeling:
Nanostructures as platform for biosensors

Richting: **master in de biomedische wetenschappen-bio-elektronica en nanotechnologie**
Jaar: **2012**

in alle mogelijke mediaformaten, - bestaande en in de toekomst te ontwikkelen - , aan de Universiteit Hasselt.

Niet tegenstaand deze toekenning van het auteursrecht aan de Universiteit Hasselt behoud ik als auteur het recht om de eindverhandeling, - in zijn geheel of gedeeltelijk -, vrij te reproduceren, (her)publiceren of distribueren zonder de toelating te moeten verkrijgen van de Universiteit Hasselt.

Ik bevestig dat de eindverhandeling mijn origineel werk is, en dat ik het recht heb om de rechten te verlenen die in deze overeenkomst worden beschreven. Ik verklaar tevens dat de eindverhandeling, naar mijn weten, het auteursrecht van anderen niet overtreedt.

Ik verklaar tevens dat ik voor het materiaal in de eindverhandeling dat beschermd wordt door het auteursrecht, de nodige toelatingen heb verkregen zodat ik deze ook aan de Universiteit Hasselt kan overdragen en dat dit duidelijk in de tekst en inhoud van de eindverhandeling werd genotificeerd.

Universiteit Hasselt zal mij als auteur(s) van de eindverhandeling identificeren en zal geen wijzigingen aanbrengen aan de eindverhandeling, uitgezonderd deze toegelaten door deze overeenkomst.

Voor akkoord,

Jacobs, Tanya

Datum: **4/01/2012**